LU NV 17-05
May 2017

Commissioning of the ΔE-E LYCCA detector array

Alexander Huusko

Department of Nuclear Physics, Lund University

Bachelor thesis supervised by Dr. Pavel Golubev and Prof. Dirk Rudolph

LUND
UNIVERSITY

Abstract

LYCCA (Lund York Cologne CAlorimeter) is a versatile detector system which provides partial and residual energy measurements together with particle tracking and identification. The detector system consists of several different types of detectors such as DSSSDs (Double-Sided Silicon Strip Detector) and CsI(Tl) detectors. LYCCA was developed for the HISPEC/DESPEC (High-Resolution In-flight SPECtroscopy/DEcay SPECtrocsopy) program within the NUSTAR (NUclear STructure, Astrophysics and Reactions) collaboration. The purpose of this bachelor project is to commission and test a part of the LYCCA detector system, the LYCCA $\Delta E - E$ telescopes. The $\Delta E - E$ telescope consists of a DSSSD and nine CsI(Tl) crystals. These telescopes are used to track and identify relativistic and charged particles. The individual detectors of the $\Delta E - E$ telescope are tested separately. The DSSSDs are tested with respect to energy spectrum, energy resolution and dead layer thickness. The CsI(Tl) detectors are tested with respect to energy spectrum. Both detector types are tested using a ^{228}Th α-source. The underlying physics of the two detectors is explained together with the setup and procedure used for the test measurements. Furthermore, the obtained results and data analysis are presented. The energy resolution of the DSSSDs was found to be between 0.49-0.77% at 8685 keV for α-particles. The dead layer thickness of the DSSSDs was estimated to be on the order of 1 μm silicon equivalent. The CsI(Tl) detector shows satisfactory results for low energy α-particles, as the main peaks of the energy spectrum are visible.

Acknowledgements

I would like to thank Dr. Pavel Golubev for supervising and helping me a lot with everything from writing this thesis to explaining the fundamental principle of the detectors.

I would also like to thank Prof. Dirk Rudolph for his support and for introducing me to Dr. Pavel Golubev and the field of nuclear physics.

Furthermore my thanks go to Dr. Luis Sarmiento for always having an open door and helping me with coding and setting up the data acquisition system.

Last but not least I want to thank my family for always supporting me throughout my studies.

Contents

1 Introduction

The universe is made up of a large amount of different types of atoms. The atomic nuclei are categorized by the number of protons and neutrons that they contain. The proton number, Z, of an atom describes which chemical element it is, while the neutron number, N, represents different isotopes of the same chemical element. The sum of the proton and neutron number is the mass number, A.

Several fields, such as chemistry and atomic physics, study on the outer most layer of the atom (electrons) and seldom have much interest in isotopes. On the contrary, nuclear physicists probe further into the atom, namely the nuclei of atoms. For nuclear physics isotopes are very important as the properties of the nuclei can vary a lot between isotopes. Figure 1 shows the nuclidic chart, which displays all known isotopes to date [1]. Along the center of the nuclide chart runs the line of stability, at which all of the nuclei are stable. Outside the line of stability lie the unstable nuclei, which are increasingly unstable the further away from the line of stability that they are. Nuclear physics studies the properties of different nuclei, all from measuring excited state energy and decay rate of nuclei to the cross section of various nuclear reactions.

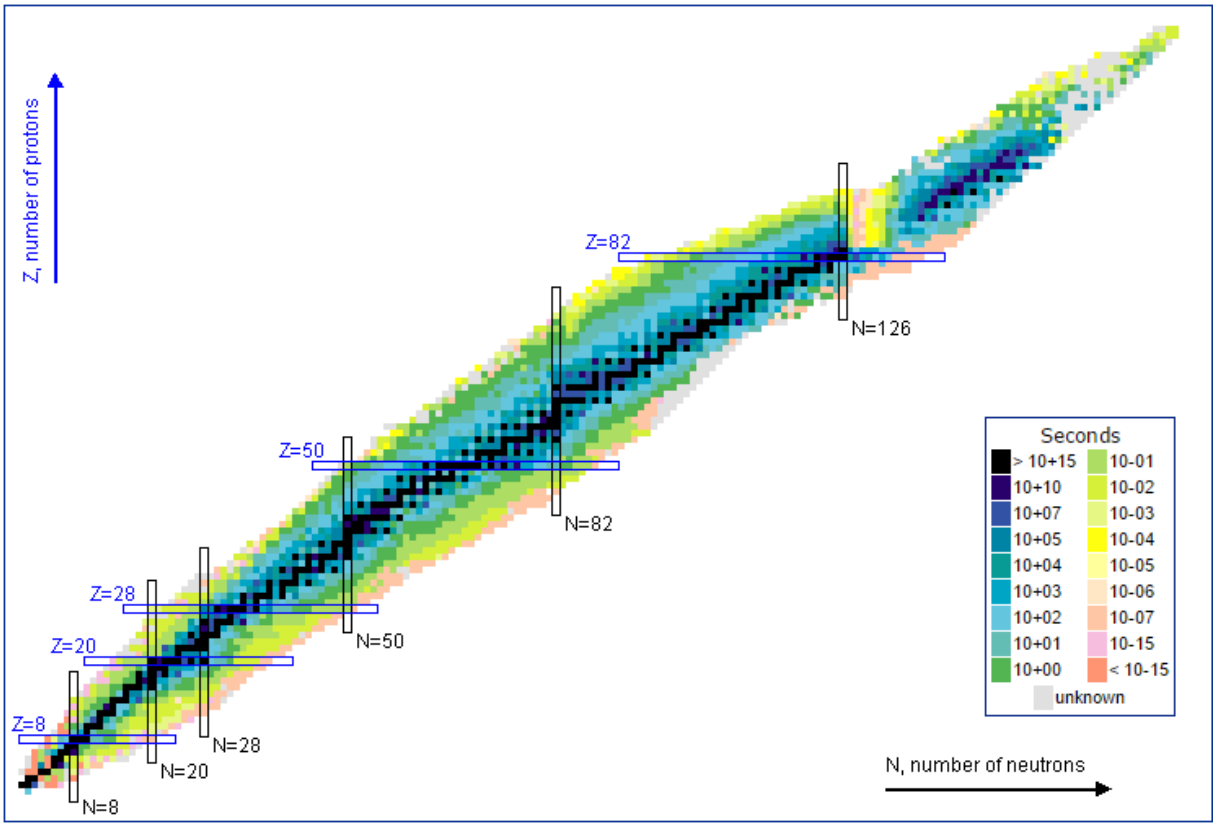

Figure 1: *Table of nuclides. The half-life is represented in colour code (which can be found in the bottom right corner) with stable nuclides marked in black [1].*

Nuclear physicists have come far and studied the properties of most nuclei which lie close to the line of stability. This means that studies in nuclear physics today usually go far from the line of stability in order to obtain new information about nuclei. This is often done by studying exotic nuclei or superheavy elements. The exotic nuclei have either a surplus of neutrons or protons, while the superheavy elements have high mass numbers. Both kinds of experiments tend to have high counting rates, and therefore it is important to make use of fast reacting detector equipment to obtain as much information as possible from each decay.

A new generation of e.g accelerators are being constructed in order to study such exotic nuclei. In Europe, new accelerators are being built at the Facility for Antiproton and Ion Research (FAIR) in Germany. The new accelerators will provide heavy-ion beam intensities which have never been reached before. This calls for new and advanced detector systems which can meet the increasing demands. The LYCCA

(Lund-York-Cologne CAlorimeter) detector system has been developed, within the HISPEC/DESPEC program (High-Resolution In-flight SPECtroscopy/DEcay SPECtrocsopy) for identification of relativistic charged particles, and will play an important role for upcoming NUSTAR (NUclear STructure, Astrophysics and Reactions) experiments at FAIR.

The LYCCA detector is a versatile system which consists of several detector elements in order to measure the Time of Flight (ToF), position and direction, partial energy loss, ΔE, and residual energy loss, E_{res}, of particles. Measuring these properties allows one to uniquely identify the proton number and mass number for particles which pass through the detector system. The LYCCA detector system also provides particle tracking before and after the secondary target. Figure 2 shows a schematic of the LYCCA detector system.

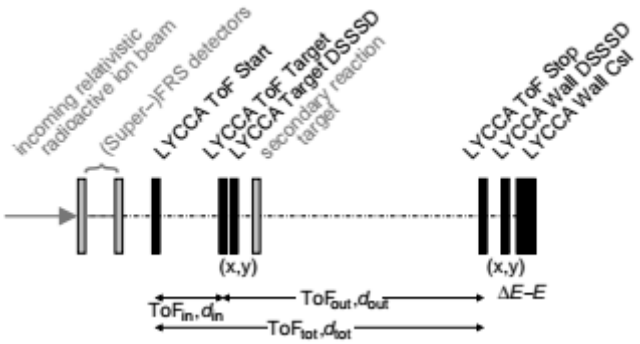

Figure 2: *LYCCA detector system with individual detector elements listed above the sketch [2].*

The ToF measurement is done by using three fast plastic scintillator detectors. The LYCCA ToF Start and Stop detectors both consist of a 27 cm diameter circular plastic scintillator membrane read out by 32 PMTs (PhotoMultiplier Tubes) each [2]. The LYCCA ToF Target detector has a smaller scintillator ring, compared to the Start and Stop detectors, of 73 mm which is read out by 12 PMTs. The LYCCA Wall DSSSD (Double-Sided Silicon Strip Detector) is used to measure the partial energy loss and has a thickness of $\approx$310 μm [2]. The DSSSD detector system also provides particle tracking information. The LYCCA CsI(Tl) detector is a scintillator detector which consists of 3x3 CsI(Tl) crystals of different thickness. The thickness of the CsI(Tl) crystals is such that relativistic particles will be stopped and deposit all of their energy inside the crystals. Each CsI(Tl) crystal is connected to a photodiode which is used to readout the scintillation light. The DSSSD and CsI(Tl) detectors are mounted together forming LYCCA telescopes. Experimental setups can contain up to 26 telescopes in order to increase the detection area. Figure 3 shows the LYCCA chamber with 3x4 LYCCA modules mounted inside the dedicated vacuum chamber.

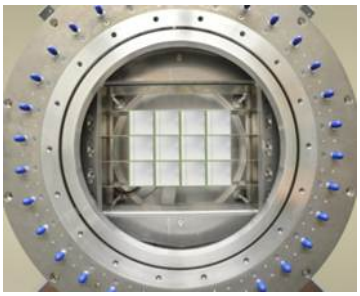

Figure 3: *The LYCCA vacuum chamber with 3x4 LYCCA modules mounted inside. 26 modules can be mounted for a larger detection area [2].*

This bachelor thesis focuses on commissioning DSSSD and CsI(Tl) detectors to make sure that they meet the requirements needed for future experiments. Each channel of the DSSSDs detectors and their individual readout system have to be tested and calibrated. The DSSSD energy resolution has to be determined in order to check if they reach the requirement specified in the LYCCA techinical design report (TDR) [9]. In addition the dead layer of the DSSSD detector will also be estimated. The CsI(Tl) detectors will also be tested to see that they meet the specified requirements for upcoming experiments.

2 Detectors

This chapter will in short explain the underlying physics of the two detector types used in the LYCCA telescopes. Furthermore, the properties of the LYCCA telescope will be described briefly.

2.1 Energy Loss of Charged Particles in Matter

Charged particles passing through matter interacts with atoms mainly by two fundamental processes, electromagnetic interaction with electrons and scattering with nuclei. The electromagnetic interaction, with the electrons in the matter, is the dominating contribution of energy loss for charged particles.

Each interaction with an electron will either excite or ionize the atom, which requires an energy in the order of electronvolt (eV). This indicates that, even for low energy particles, it takes a large amount of interactions before the charged particle has lost a significant amount of energy. The Bethe-Bloch formula [3], as seen in Equation 1, describes the mean energy loss per unit length of charged particle passing through the matter.

$$-\frac{dE}{dx} = \frac{4\pi}{m_e c^2}\frac{nz^2}{\beta^2}\left(\frac{e^2}{4\pi\epsilon_0}\right)^2\left[ln\left(\frac{2m_e c^2\beta^2}{I(1-\beta^2)}\right) - \beta^2\right], \tag{1}$$

where E is the energy of the particle, x is the particle travel distance, m_e is the electron rest mass, c is the speed of light, n is the electron density, which is given in Equation 2, z is the charge of the particle (expressed in electron charge), β is the particle speed expressed in c, e is the electron charge, ϵ_0 is the vacuum permittivity and I is the mean ionization potential of the medium.

$$n = \frac{N_A \cdot Z \cdot \rho}{A \cdot M_u}, \tag{2}$$

where N_a is the Avogadro number, Z is the atomic number of the material atoms, ρ is the material density, A is the relative atomic mass and M_u is the molar mass constant.

Equation 1 was often referred to as the Bethe formula, until the mean ionization potential described by Bloch was introduced in 1933, as seen in Equation 3, after which it is called the Bethe-Bloch formula.

$$I = Z \cdot 10 \text{ eV}, \tag{3}$$

where Z is the atomic number of the material atoms.

For low energy particles, $\beta << 1$, the Bethe-Bloch formula can be given as:

$$-\frac{dE}{dx} = \frac{4\pi}{m_e v^2}nz^2\left(\frac{e^2}{4\pi\epsilon_0}\right)^2\left[ln\left(\frac{2m_e v^2}{I}\right)\right], \tag{4}$$

where v is the speed of the particle.

2.2 DSSSD

The Double-Sided Silicon Strip Detector (DSSSD) is a semiconductor device used for measuring both the partial energy loss ΔE and the position in the x-y plane of incident particles. The DSSSD is also used in a set of two or more in order to provide a particle tracking system.

A semiconductor is a crystal which has properties similar to insulators, but also similar properties to conductors. Semiconductors and insulators differ from conductors in that they have a filled valence band and an empty conduction band, while conductors have electrons in their conduction band. This allows the conductors to freely conduct electricity. For semiconductors and insulators to conduct electricity, the electrons have to be excited from the valence band into the conduction band, across the band gap. The difference between a semiconductor and an insulator is the energy width of the band gap. Figure 4 shows the band structure of the different materials. While the definition of maximum band gap for a semiconductor is not firmly defined, it is usually in the order of a few eV. Insulators have wider energy gaps than semiconductors. The relatively small band gap of semiconductors allows electrons to be thermally excited across the band gap, allowing the material to conduct electricity at room temperature.

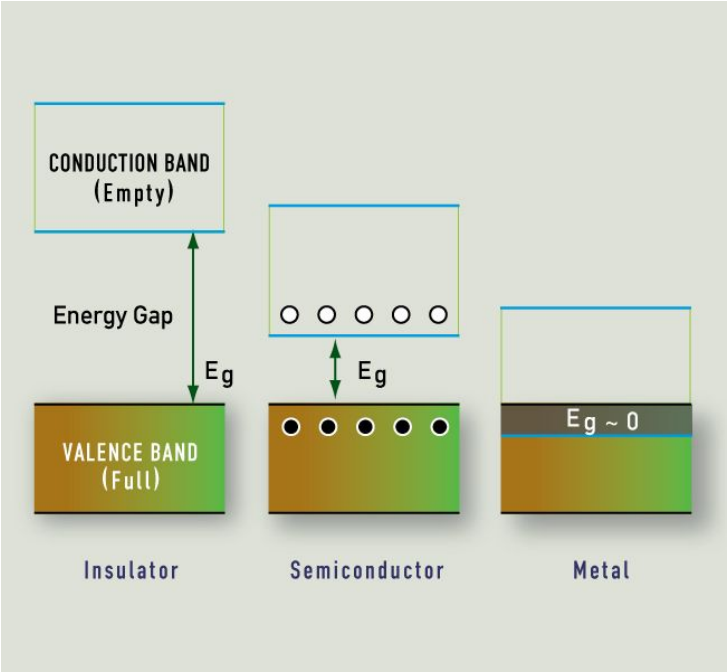

Figure 4: *Band structure of an insulator, a semiconductor and a conductor [4].*

Intrinsic/pure semiconductors are made up of atoms with four valence electrons or combinations of atoms which results in a similar structure such as III-V. Each atom binds one electron to each neighbouring atom in covalent bond, resulting in a tightly bound system and a filled valence band. III-V is an example of a material which has three and five valence electron materials in which the three valence material borrows an electron from the other atom. This allows the material to obtain fill the valence band just as for the four valence electron material. Semiconductors can be doped by adding atoms with either three (p-doped) or five (n-doped) valence electrons. This will result in either a shortage or surplus of one electron in the bond with the adjacent atoms. This process is called "doping of a semiconductor", which adds either donor (five valence electron atoms) or acceptor (three valence electron atoms) energy states to the crystal. The extra electrons or missing electrons (referred to as holes) added by doping will reside in these states. Figure 5 shows the band structure of a p-doped and n-doped semiconductor.

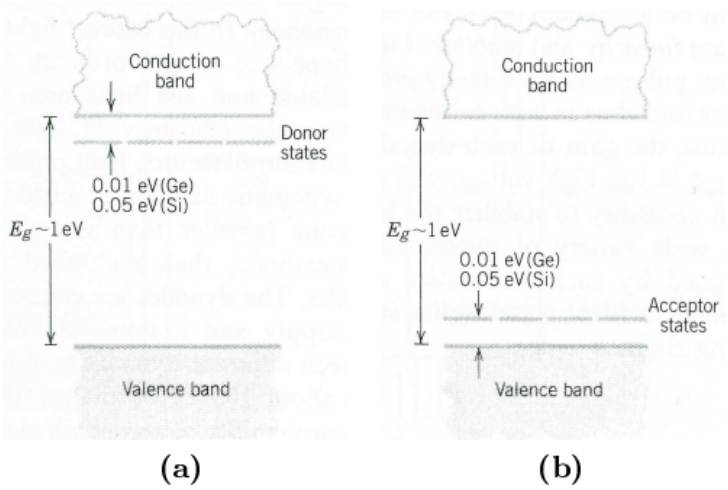

Figure 5: *Band structure of: (a) n-doped semiconductor and (b) p-doped semiconductor. Note how close the donor and acceptor states are to the conduction and valence bands [5].*

The donor and acceptor states are located very close to the conductor or valence bands. Therefore, the electrons and holes are easily excited into the conduction and valence bands respectively. More practical properties can be obtained by putting a p-doped semiconductor together with an n-doped semiconductor

and creating a so called pn-junction (they are not simply put together, but more advanced technological methods are used to create pn-junction structure). The extra electrons from n-type semiconductor will diffuse towards the p-type and the holes diffuse towards the n-type. The electrons will then fill the holes, filling the valence band. Since both types of semiconductor were initially neutral the movement of the charges will results in a in-built electric field across the crystal. In addition to the electric field, a charge neutral zone, called depletion region is created along the pn-junction. The depletion region is important for detecting ionizing particles. A reverse bias can be applied in order to deplete the entire crystal.

When incoming radiation deposits its energy into the depletion region, electron-hole pairs are created which will then move in the electric field towards the corresponding anode and cathode, resulting in a signal. The advantage of semiconductor detectors is the average energy required to create free charge carriers (electron-hole pairs) compared to other detector types. The average energy required to create an electron-hole pair for semiconductors is on the order of a few eV, while the average energy required for a gas is tens of eV and scintillators require even more energy. This means that semiconductors will have more charge carriers created per energy unit, resulting in a larger signal to noise ratio. The energy required for silicon at room temperature is 3.62 eV. The intrinsic energy resolution, R, can be calculated as:

$$R = 2.35\sqrt{\frac{Fw}{E}}, \tag{5}$$

where F is the Fano factor, w is the average energy for electron-hole creation and E is the energy of the incident radiation. The Fano factor for silicon is 0.12, which implies a good resolution for this type of detectors.

For manufacturing a LYCCA type DSSSD a n-doped high resistivity silicon wafers are used as a base. A heavily doped p^+ layer of boron is deposited into the front side of the crystal (p-side), while a heavily doped n^+ layer of arsenic is deposited into the rear side of the crystal (n-side). The boron doping creates a pn-junction with a depletion zone extending almost exclusively into the undoped silicon crystal. A reverse bias of 50 V is applied in order deplete the entire silicon crystal, to increase the radiation sensitive volume over the entire wafer. Readout electronics are connected, directly to the heavily doped boron (p-side) and arsenic (n-side) layers with thin layer of aluminium metalization. In order to provide discrete position measurement the p- and n-side are structured in 32 parallel strips on each side of the detector. The strips on the p-side are placed orthogonal to the strips on the n-side, and together they form a discrete grid of 1024 pixels for position measurements in the x-y plane. Figure 6 shows a schematic image of a DSSSD.

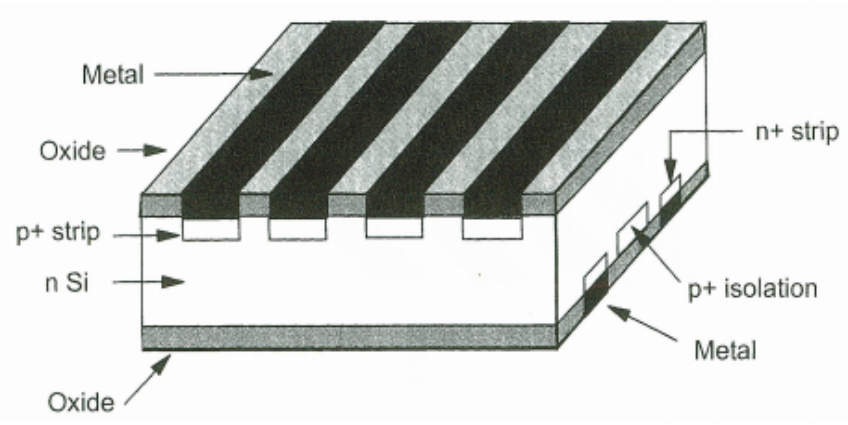

Figure 6: *Scheme of a Double-sided silicon strip detector [6].*

To avoid rectifying junction with additional depletion zone, due to direct contact between metal and semiconductors, the semiconductor is heavily doped under the metalization. Highly doped silicon together with metalization and passivation layer form so called dead layer which is unsensitive to incoming radiation. The effect of dead layer will be discussed later.

The high energy resolution of the DSSSD, combined with its good position measurement makes it a favourable detector choice for particle identification and tracking for LYCCA.

The silicon wafers used for LYCCA telescopes are ion implated, passivated with silicondioxide (SiO_2), and operated fully deplted with floating guard rings. They have been obtained from RADCON limited [11]. The 300-320 μ silicon wafers are squared shaped 60.1 mm x 60.1 mm, with an active area of 58.5 mm x 58.5 mm. The width of the p-side strips is 1.8 mm with an interstrip SiO_2 isolation of width 30 μm. The n-side strip width is 1.63 mm with an interstrip SiO_2 isolation of 200 μm. The leakage current after production range between 5 and 10 nA per strip. Each strip has a capacitance of 33 pF at full depletion which is typically reached at 50 V. RADCON limited found that the dead layer thickness is $\sim$1.0 μm on the p-side and $\sim$2.0 μm on the n-side (both thicknesses are expressed in silicon equivalent).

2.3 CsI(Tl) Detector

The CsI(Tl) detector block consists of nine CsI(Tl) crystals arranged in a 3x3 array. The CsI(Tl) crystals are on the order of a few cm in thickness in order to stop all the relativistic ions in experiments with LYCCA detectors. The CsI(Tl) detector is mounted behind the DSSSD detector in the LYCCA telescope. The CsI(Tl) detector is an inorganic scintillator detector which is readout by a photodiode.

Scintillators are insulators, meaning that they have a filled valence band and an empty conduction band. When radiation passes through a scintillator, it excites the atoms and molecules of the scintillator. The atoms and molecules later (in the order of ns) decay to their original state, through recombination with the hole created in the excitation, emitting photon(s) in the process. The photons can then converted into a signal using either a photodiode or photomultiplier tube (PMT). However, scintillators need to have self-transparency, meaning that they do not absorb the scintillation photons. In case of a pure scintillator, the photons sent out will have energies matching the band gap of the scintillator. These photons can with high probability be absorbed by molecules in the ground state, causing excitation and then deexcitation again. Thus the material would not efficiently transport the photons to the light readout system. In order to achieve the self-transparency, impurities are introduced. These impurities create states, called activator states, in the forbidden region between the valence band and the conduction band. Figure 7 shows the band structure of an inorganic scintillator.

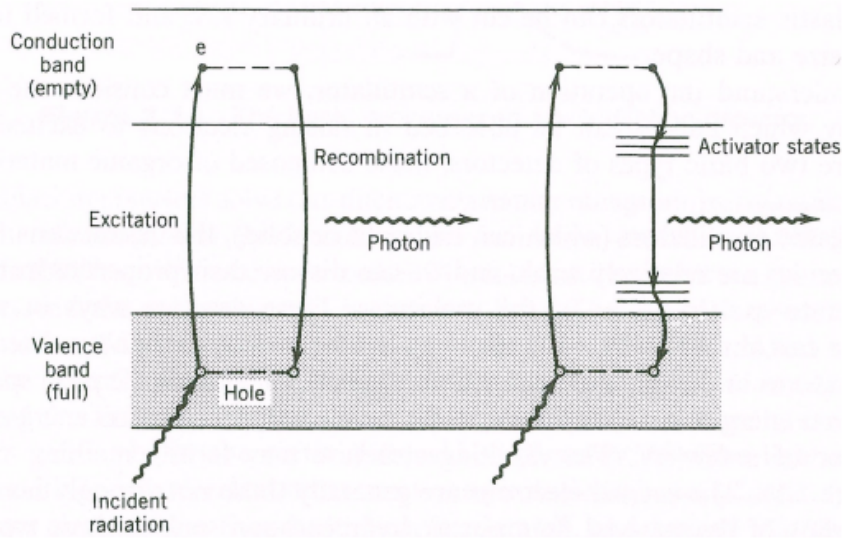

Figure 7: *Band structure of an inorganic scintillator crystal. The left side shows a pure scintillator crystal, and the right side shows a scintillator crystal with impurities [5].*

These states are unoccupied, which means that when the molecules are to deexcite back to the ground state they can go through the unoccupied states in the forbidden region. The emitted photons have energies smaller than the energy of the band gap meaning that ground state molecules can not absorb them. Furthermore, the intermediate energy states are unoccupied, which means that no part of the scintillator will absorb the photons, thus making the scintillator self-transparent. The wavelength shift of the photons is often a benefit of itself as it helps match the emission spectrum to the absorption spectrum of photodiodes or photoelectric materials used in PMTs. The resolution of scintillator detectors is worse

compared to semiconductor detector. However, scintillators are cheaper and can be made in larger sizes, making them beneficial when it comes to having large detectors. Also, scintillators material has a higher stopping power than semiconductor materials. Having large scintillator detectors is practical as they can reach the stopping power required to stop high energy particles.

The CsI(Tl) crystals used in the LYCCA telescopes have the front side dimensions 19.4 mm x 19.4 mm, and a thickness of 10 mm (short version) or 33 mm (long version). The CsI(Tl) crystals have been obtained from Amcrys-H Ltd [12]. The typical Tl concentration is 0.08-0.10 mol%. A pyramidal waveguide of 5 mm (short version) and 7 mm (long version) is mounted to the back of each CsI(Tl) crystal in order to guide the light to the photodiode. The back side of the waveguide has the dimensions 10.4 mm x 10.4 mm. To minimize the incoming particle energy loss each crystal is covered by a 12 μm aluminium foil on the front side. All other sides are covered by ESR (Enhanced Specular Reflector) which increases the photon collection by the photodiode. In order to reject optical cross talk between adjacent crystals additional layer of 12 μm aluminium foil is inserted between the CsI(Tl) detectors.

The photodiodes, used to readout LYCCA CsI(Tl) detectors, are 10.6 mm x 11.6 mm and 0.3 mm in size and are supplied b y RADCON Ltd.The photodiodes have a quantum efficiency of $\sim 72-86\%$ at 560 nm, which is the peak position of the CsI(Tl) emission spectrum. The photodiode has a operating voltage of 35 V, a leakage current of 1-2 nA and a capacitance of 38-40 pF (at full depletion).

2.4 LYCCA Telescope

Each LYCCA telescope consists of one DSSSD and nine CsI(Tl) detectors arranged in array of 3x3 CsI(Tl) crystals with photodiode readouts. The CsI(Tl) detectors are mounted inside a brass frame. The photodiode signal is readout using coaxial cables for each CsI(Tl) crystal block. To minimize dead area between detectors the DSSSD is directly mounted onto the LYCCA telescope frame with integrated printed circuit board in order to transport the signal to the charge sensitive preamplifier by means of flat ribbon cables. Figure 8 shows the LYCCA telescope components.

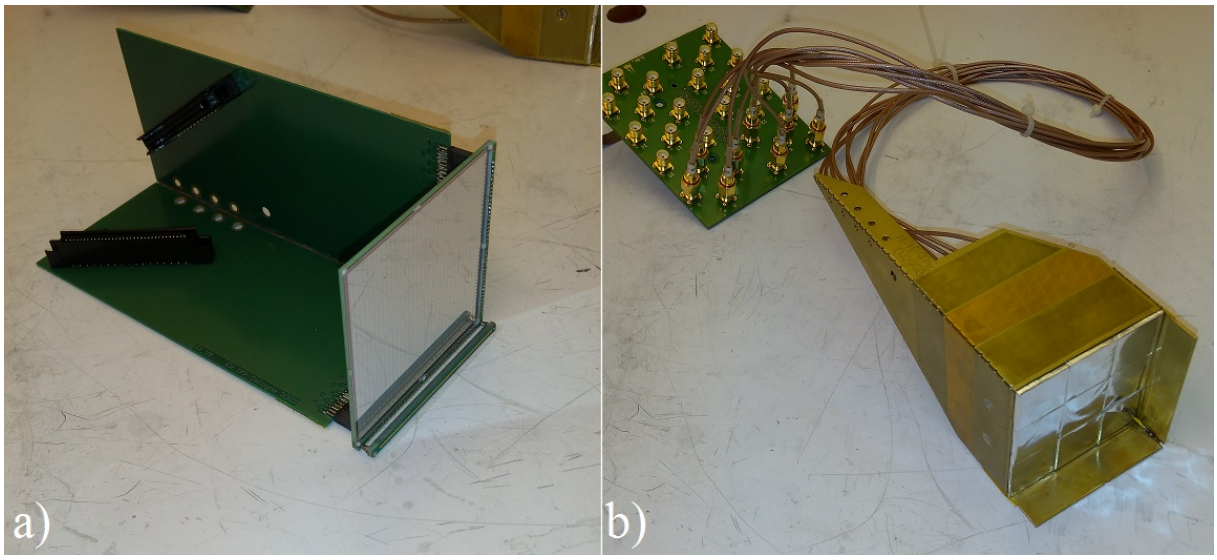

Figure 8: *a) shows the DSSSD and frame used in LYCCA telescopes. In the back one can see the readout connection for the DSSSD. b) shows the CsI(Tl) detectors with the brass frame and custom-made coaxial-to-flat ribbon cable converter.*

Each frame of the LYCCA telescope is detachable, making it possible to test the DSSSD and CsI(Tl) separately as well as making exchange or repair parts on either frame easier.

3 Detector Testing Experimental Setup

Testing the DSSSD and CsI(Tl) detectors requires a dedicated experimental setup. This chapter will briefly explain the different components used in the detector test setup and a data acquisition system

(DAQ). The DAQ used to test the detectors is a simpler version of the readout system developed for future experiments at FAIR. Figure 9 shows the detector test setup.

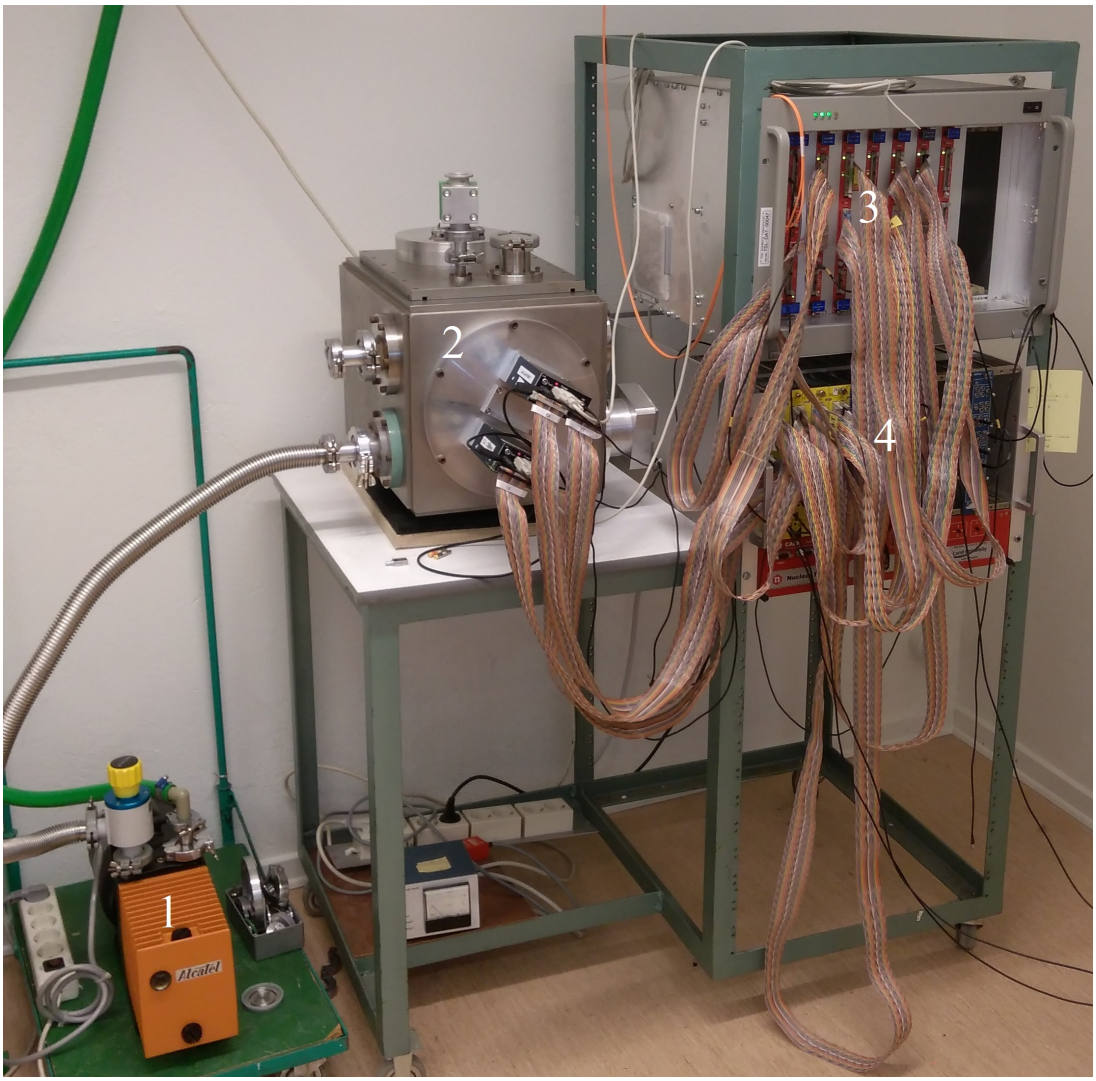

Figure 9: *Experimental setup used for testing the LYCCA DSSSD and CsI(Tl) detectors in Lund. 1. vacuum pump, 2- vacuum chamber, 3- VME and readout electronics, and 4- NIM electronics: shapers, high-voltage generator and trigger logics.*

A ^{228}Th source is used in order to test and calibrate the DSSSD and CsI(Tl) detectors as well as determine their energy resolution.

3.1 Vacuum Chamber

Both types of detectors were tested in a vacuum chamber using a ^{228}Th α-source. Vacuum is needed in order for the α-particles to reach the detector, as well as avoiding energy loss due to air ionization on its way to the detectors. The vacuum chamber is made of stainless steel and has several ports which can be used in order to connect vacuum pumps, vacuum gauges and feedthroughs. The vacuum chamber is equipped with three feedthroughs for signal transportation to the preamplifiers. Figure 10 shows the outside and inside parts of the vacuum chamber as it is being used in the measurements.

Figure 10: *a) shows the outside of the vacuum chamber and b) shows the inside of the vacuum chamber. 1- air valve, 2- vacuum feedthrough and preamplifiers, 3- vacuum pump, 4- mounted source, 5- DSSSD and 6- flat ribbon cable.*

The top lid of the vacuum chamber has a valve, used to let in air into the chamber. There is also a glass window mounted on the top of the vacuum chamber, which is covered by a removable metal top which completely seals the chamber and prevents light from entering the chamber.

3.2 Data Acquisition system

The DAQ is a central part of the experimental setup as it enables data collection from all channels simultaneously in event-by-event mode. These events can then be on-line or off-line analyzed in order to obtain recorded information.

3.2.1 DAQ Setup

The experimental setup uses two CSP-32 (multichannel charge sensitive preamplifier) units and four MSCF-16 (shaping, amplification and timing with leading edge discriminator) to readout the DSSSDs (p- and n-side) and CsI(Tl) detectors. For digitization two CAEN V785 (32 channel peak sensing ADC) are used along with two CAEN V775 (32 channel TDC) [10]. The digitizing units are controlled using a SBS 620-3 PCI-to-VME adapter unit. The VME control unit is connected to a master computer, using optic fiber cable, from which the DAQ is controlled. The DAQ software is developed in C++ using ROOT libraries [7]. The trigger request is an OR between every CsI(Tl) channel for its measurements and as an "OR" between every DSSSD p-side channel for its measurements.

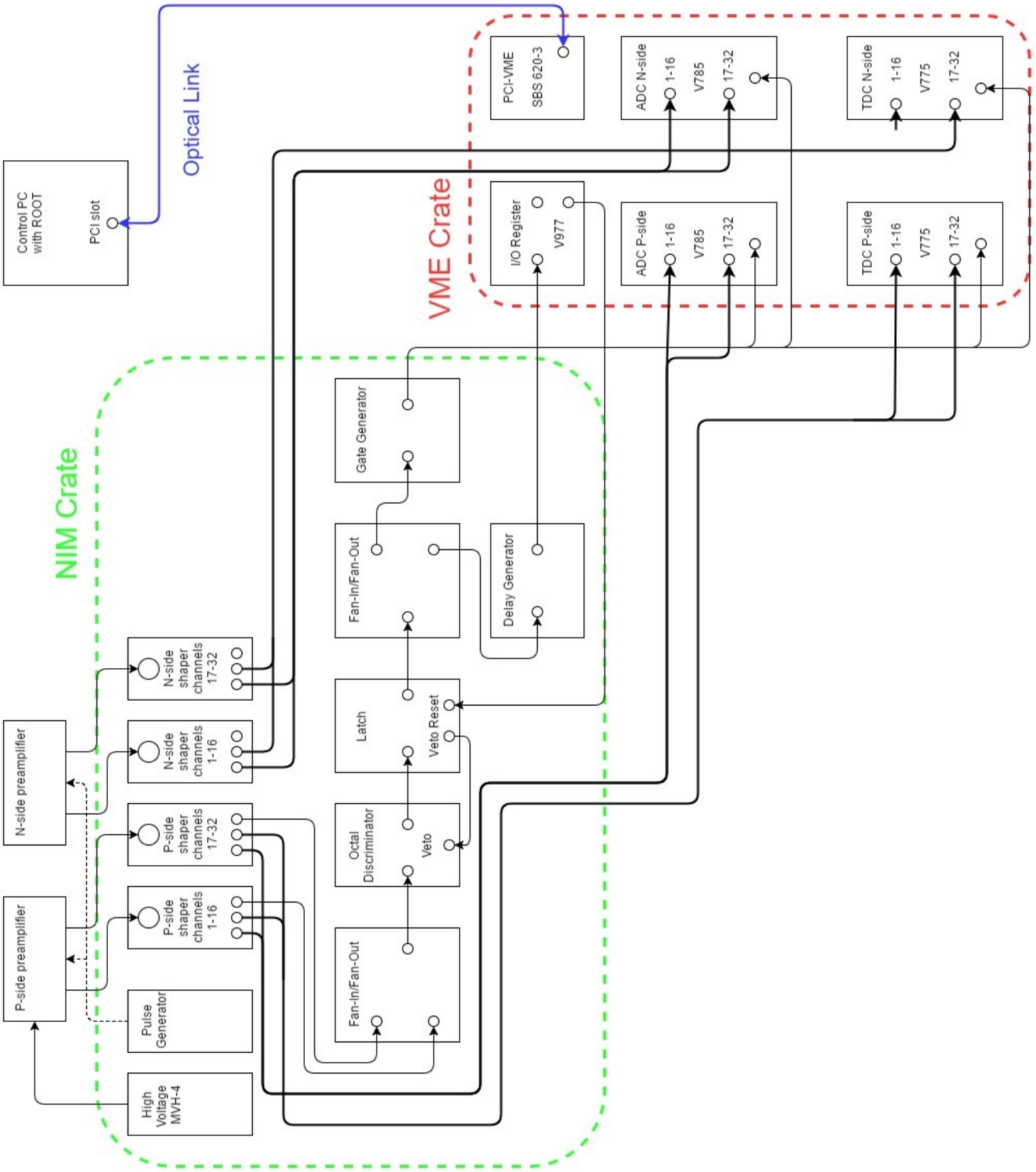

Figure 11: *Block diagram of the DAQ system.*

3.2.2 Signal Amplfication and Shaping

To process DSSSD and photodiode signal the CSP-32 charge sensitive preamplifier was developed at the University of Cologne [2]. The CSP-32 was designed to cover a wide energy range of signals from both DSSSDs and photodiodes coupled to CsI(Tl) detectors. The preamplifiers can be configured to cover energy range up to 4 GeV range. The preamplifier uses a set of stages to process the input signal. The first stage is a charge sensitive loop, followed by a passive pole-zero cancellation and attenuation stage which ends with a balanced differential output buffer. The preamplifier has a conversion factor of 50 V/pC.

The amplification and shaping is done using MSCF-16 NIM modules [8]. Each module consists of 16 channels and is equipped with a trigger, pole-zero cancellation, shaping and amplification signal processing parameters which can be set per channel or in common for all channels within the module. These settings can be adjusted on the module front panel or by using dedicated software. Amplification factor and threshold can also be set manually on the front panel. Each module has a set of jumpers which sets the amplification factor. These jumpers can be exchanged to reach a desired energy range. The positioning of the jumpers also determine polarity of the incoming signal, which has to be set for the p and n side of the DSSSDs. In case of the input signal polarity missmatching the output signal will be distorted, as seen in Figure 12. The pulse shaper uses the CR-RC method to perform semi-Gaussian shaping of the input signal. This method also filters out high frequency components and gives an optimal signal-to-noise ratio.

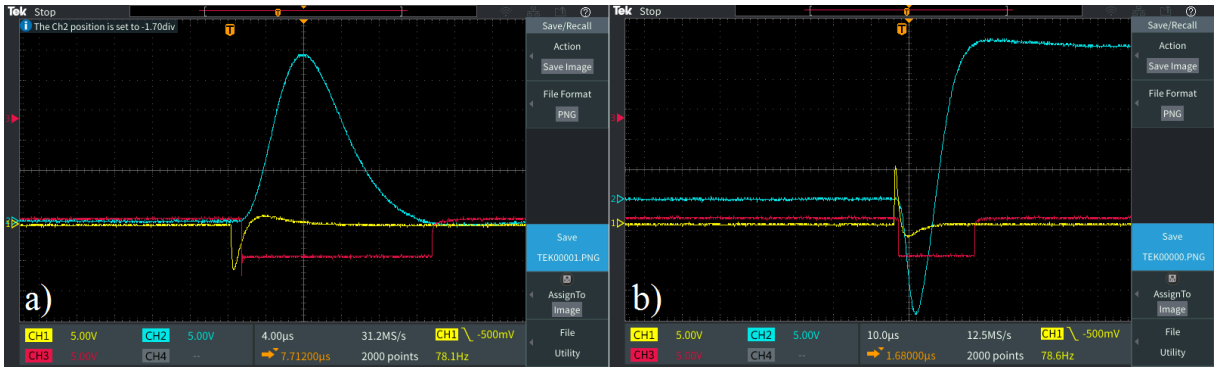

Figure 12: *a) shows a shaped signal with matching input polarity and b) shows a shaped signal with mismatching input polarity. The blue lines represent the shaped energy signal, yellow lines represent the trigger and red lines represent the ADC gate.*

Besides shaping and amplifying signal, the MSCF-16 module also provides timing signal based on Leading Edge (LE) discriminator. Each MSCF-16 module also generates a common trigger output signal as OR of all channels. This trigger signal can be used to create a common gate for ADC or TDC units.

3.2.3 Signal Converters

In order to digitize the output signals amplitudes and timing signals from the MSCF-16, the CAEN V785 ADC and the CAEN V775 TDC VME modules are used. Each module can process 32 channels simultaneously and use a common gate for all channels. The ADC digitizes the amplitude of the incoming pulse and stores the data in the output buffer for later readout.

The TDC produces a digital output which corresponds to the time difference between the individual input signals and the gate which is provided to the TDC externally. There are two modes of TDC operation: common start and common stop. The common start mode starts the time measurement at the arrival of the gate and ends with the time signal from the MSCF-16. The common stop starts with the time signal from the MSCF-16 and ends with the arrival of the gate. Figure 13 shows an example of signals arriving according to the common stop. The mode is configured using the drivers in the computer which is connected to the VME crate. The TDC mode of operation is defined by arriving signal sequence. The delay unit can be used to align signals in time and match the desired TDC mode. The TDC range can be set from 140 ns and up to 1200 ns.

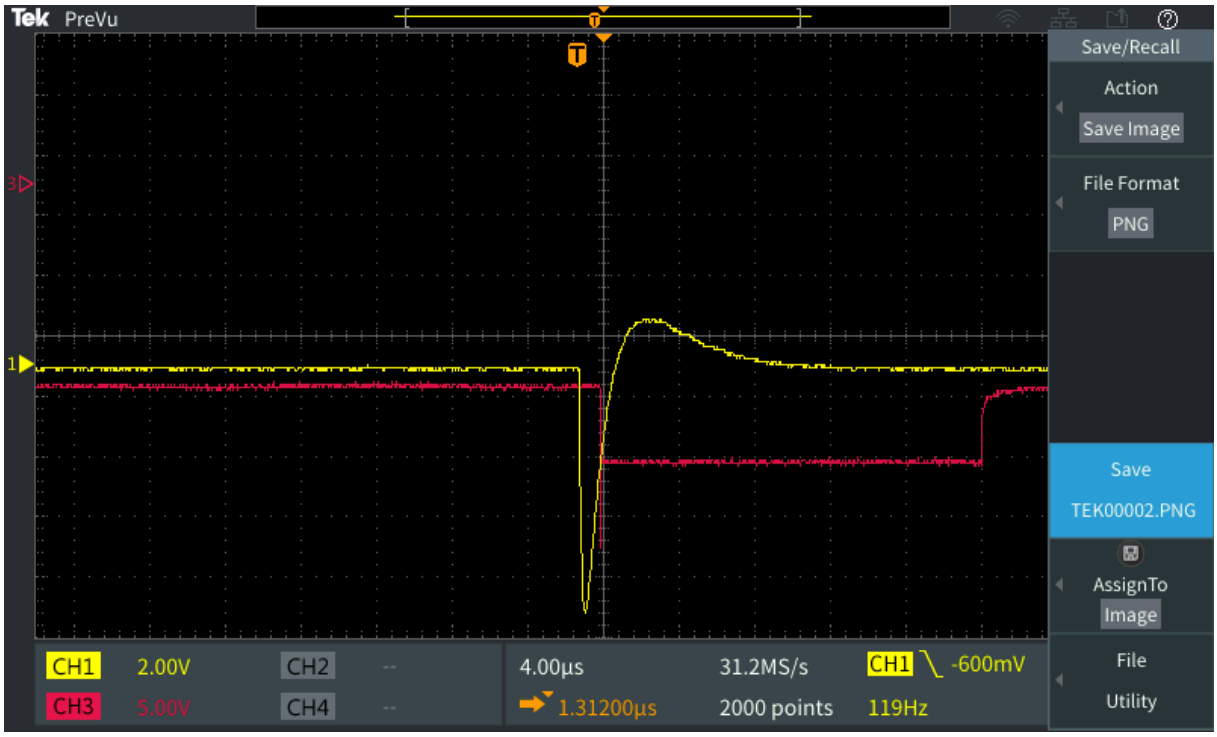

Figure 13: *Trigger (yellow) arriving before the gate (red). The time reference of a signal is determined by the falling edge.*

Both the ADC and TDC require finite time, 5.7 μs, to convert signals into digital form. This time is referred to as conversion time and has to be taken into account during module readout. During this time the ADC and TDC can not take another input. If another input enters the ADC/TDC while it is still processing a previous signal a pile up happens and the collected data is distorted. In order to prevent pile up from happening, a VETO signal is introduced into the DAQ. When an input signal is registered, the trigger is sent to a latch which produces a VETO and sends the trigger forward to a gate generator, which produces a gate for the ADC and TDC. The VETO will block out any other incoming triggers. This means that the ADC and TDC will not record new data. The trigger is also forwarded to a delay generator which delays the signal by a few μs and then feeds the signal into the I/O (input/output register) unit to initiate ADC and TDC readout by the DAQ computer. When the readout process is finished a signal is sent back from the DAQ computer, via the I/O unit, to reset the latch, allowing a new trigger to enter the system.

4 Measurements, Data Analysis and Results

This chapter will go through the measurements done to test the DSSSDs and CsI(Tl) detectors. The analysed data will then be presented and results will be discussed in the summary chapter. The LYCCA telescopes were disassembled and individual parts were tested separately. The DSSSDs will be tested regarding 2-D hit pattern, energy resolution and dead layer on the p-side. The CsI(Tl) will be tested for response on α-particles from a ^{228}Th α-source. Appendix A and B shows the scripts used for the data analysis.

4.1 DSSSD Testing

The DSSSD measurements were performed using a vacuum compatible ^{228}Th α-source. The emitted α-particles were fully stopped by the 300-310 μm silicon, which made it a good source for energy measurements of the DSSSDs. The source was placed 95 mm away from the DSSSD, and was centered to the front of the detector, as seen in Figure 10. Before each measurement the vacuum champer was pumped to 10^{-3} mbar and then a reverse bias of 50 V was applied to the DSSSD. The ^{228}Th α-source measurements were acquired and analyzed with respect to ^{228}Th energy spectrum, energy resolution and dead layer estimation.

4.1.1 2D Hit Pattern

One of the ways to scan a detector quickly is to plot a 2D hit pattern. 2D hit patterns can be used to identify malfunctioning channels. The way this can be seen is that there will be strips missing in the 2D hit pattern, as shown in Figure 14. Such channels can then be inspected.

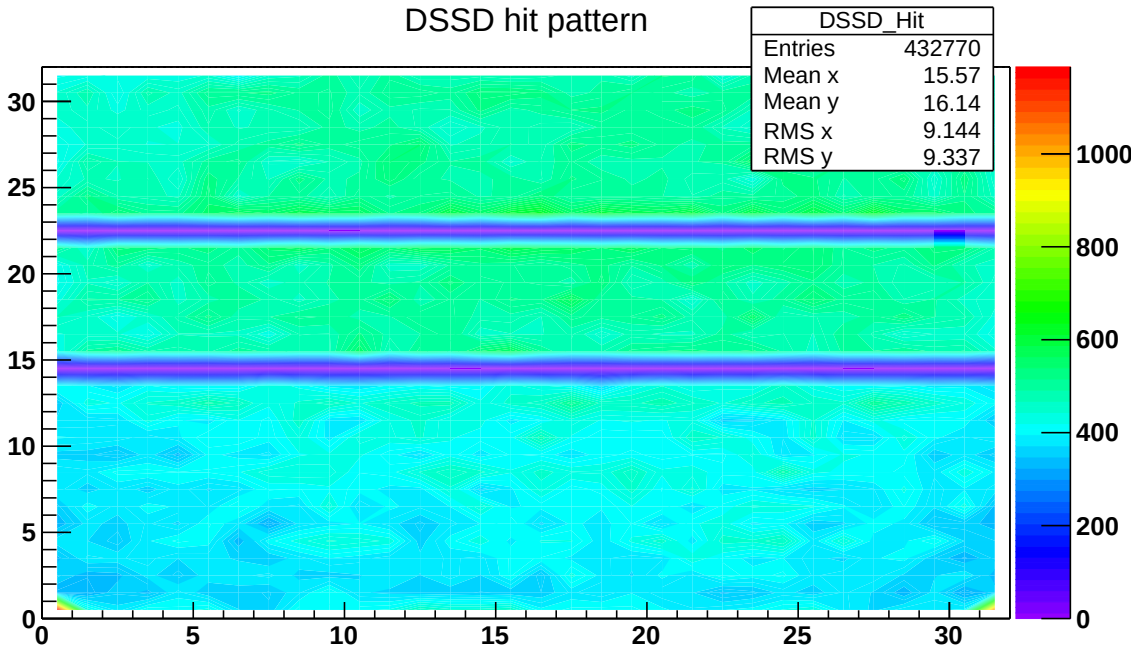

Figure 14: *2D hit pattern with two offline n-side channels for DSSSD "D20-15" measurement.*

In order to check that the DAQ and software maps the channels correctly, a thin plastic strip was placed in front of the detector to shadow the incident α-particles. The 2D hit pattern will show a clear mark from the strip, as shown in Figure 15.

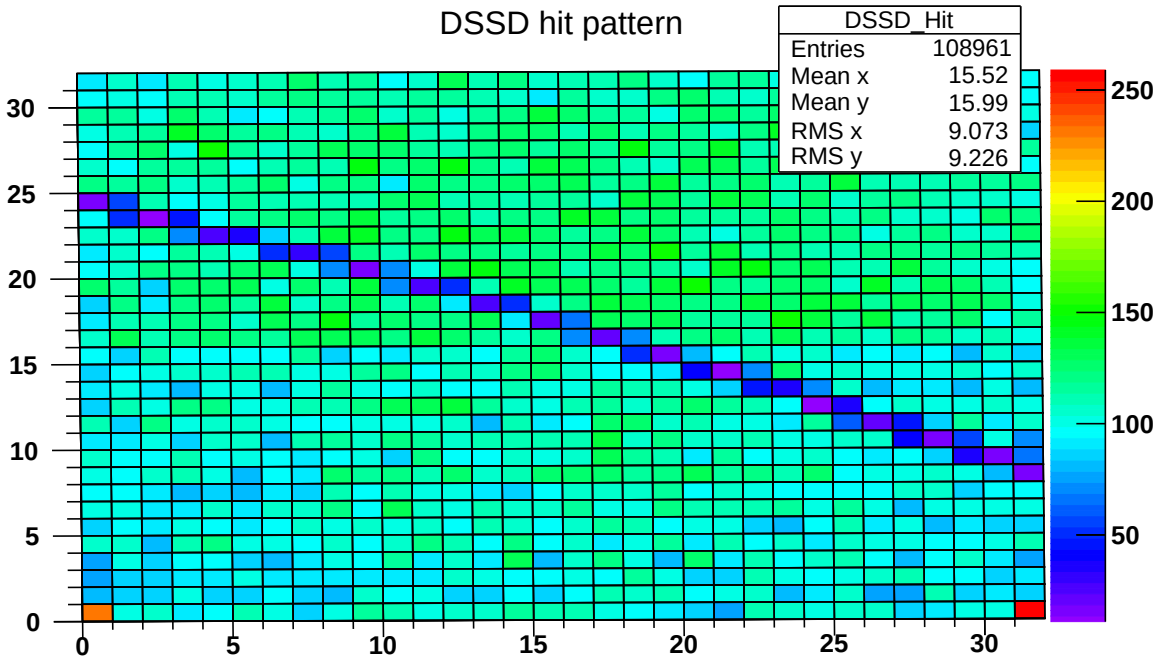

Figure 15: *2D hit pattern for a DSSSD detector with a plastic strip placed in front of it.*

The 2D hit pattern agrees with the position of the plastic strip which confirms that the DAQ and software are properly set up.

4.1.2 ^{228}Th Energy Spectrum

The DSSSD energy calibration was done using ^{228}Th α-source. The energies and relative intensities are given in Table 1. Figure 16 shows the raw energy spectrum for one measurement with gaussian fits for the six peaks.

Table 1: *Energy and relative intensity of the strongest α-particle peaks from ^{228}Th α-source [13].*

Isotope	Energy [keV]	Relative Intensity
^{228}Th	5423.15	0.722
^{228}Th	5340.36	0.272
^{224}Ra	5685.37	0.949
^{220}Rn	6288.08	0.999
^{216}Po	6778.3	~ 1.00
^{212}Bi	6050.78	0.251
^{212}Bi	6089.88	0.098
^{212}Po	8784.86	0.64

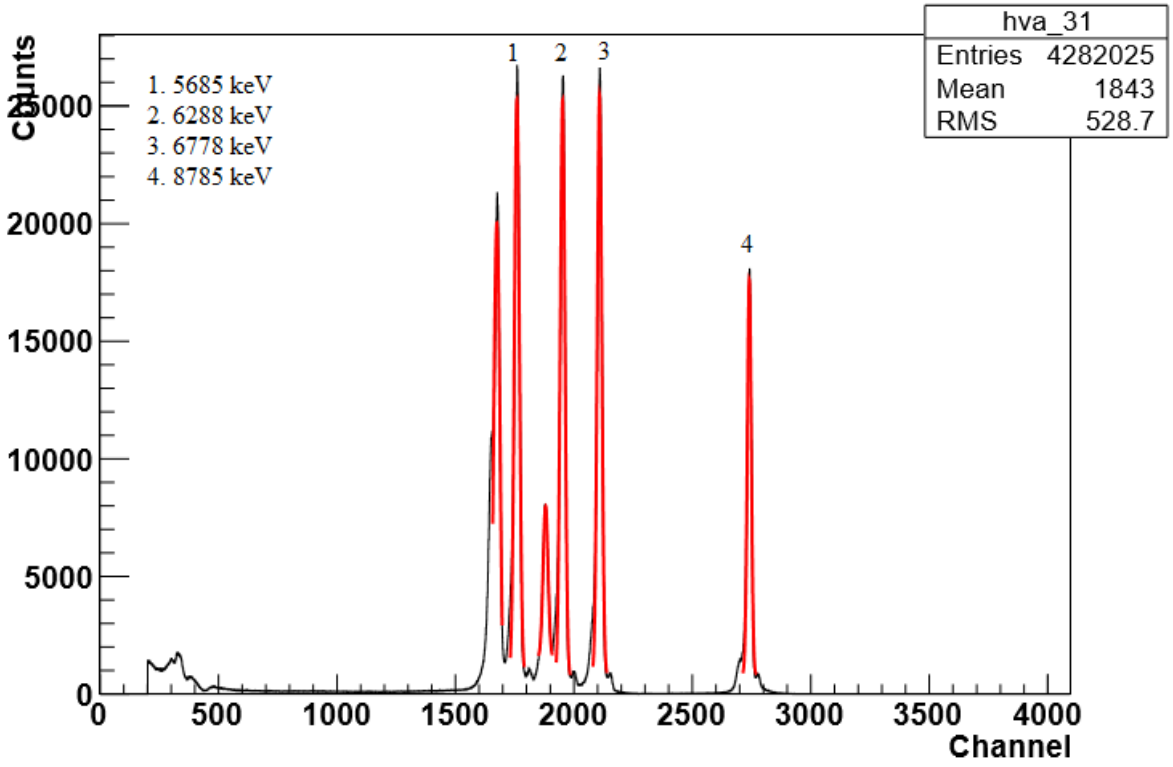

Figure 16: *Raw energy spectrum for DSSSD "PS32NS32-H" Channel 31 using a ^{228}Th α-source. Gaussian fits of the peaks are marked in red. Energies are listed in the top left corner for single peaks.*

Figure 17 shows the calibrated energy spectrum for one DSSSD energy measurement. The shape difference between the uncalibrated and calibrated spectrum is due to rebinning.

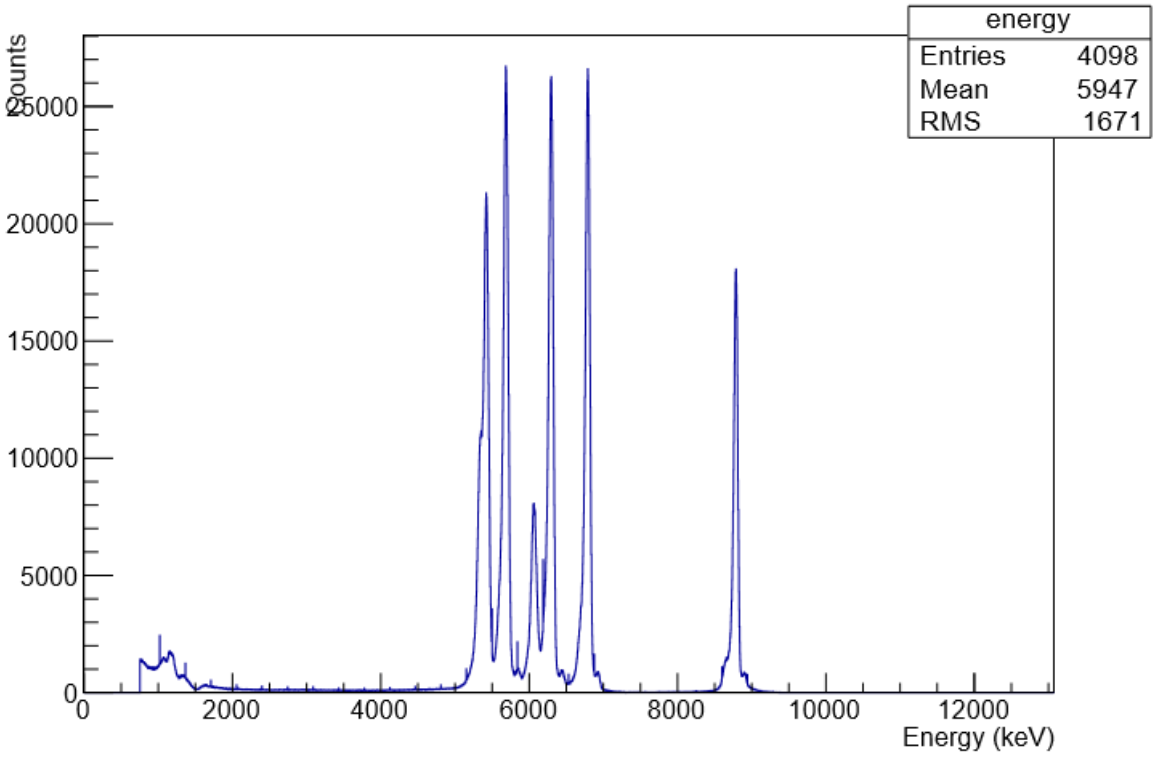

Figure 17: *Calibrated energy spectrum for DSSSD "PS32NS32-H" Channel 31 using a* ^{228}*Th* α*-source.*

After the calibration procedure, the relative intensity and energy of each peak were compared to the data in Table 1. Table 2 shows the measured energies and relative intensities of the ^{228}Th α-source peaks.

Table 2: *Measured energy and relative intensity of each peak for the DSSSD "PS32NS32-H" using a* ^{228}*Th* α*-source. *Convolution between the two peaks.*

Isotope	Energy [keV]	Relative Intensity
^{228}Th*	5413(97)	1
^{224}Ra	5681(71)	0.9448(16)
^{220}Rn	6290(76)	0.9077(16)
^{216}Po	6782(68)	0.8906(15)
^{212}Bi*	6061(66)	0.3394(8)
^{212}Po	8780(59)	0.5620(11)

Comparing the results in Table 2 to the reference data in Table 1 one can see that the energies lie very close and that the ^{228}Th and ^{212}Bi has energies which lies in between their two convoluted peaks. As for the relative intensity it agrees well for ^{224}Ra and the convoluted ^{212}Bi but other than that the values fall short of the reference values. This can be due to the overlap between peaks and the method used to calculated the peak intensity. The peak intensity is calculated by summing up the total area under each peak. Since there is an overlap some counts from neighbouring peaks will be added when calculating the peak intensity. This overlap can be seen in Figure 17 in the 5000-7000 keV range.

4.1.3 Energy Resolution

In order to estimate the energy resolution of each DSSSD detector, the gaussian fits for the uncalibrated energy spectrum were used along with the energy calibration, see Figure 16. Figure 18 shows a strip-by-strip energy resolution of DSSSD "PS32NS32-H" p-side.

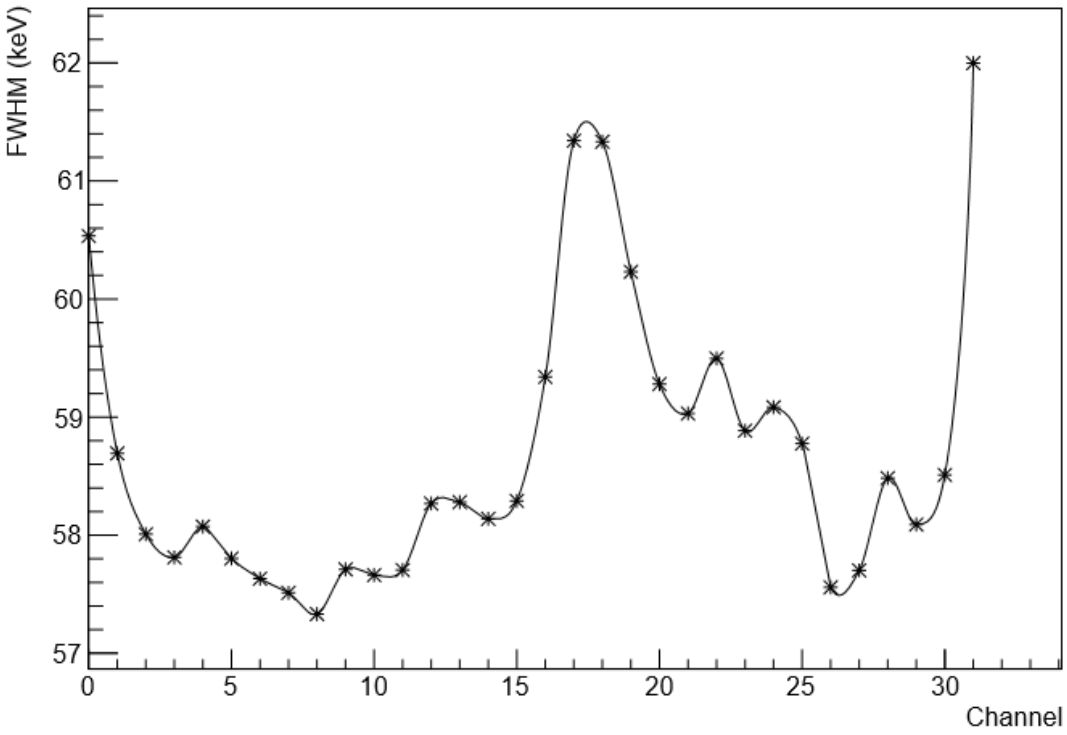

Figure 18: *Energy resolution of the 8784.86 keV* ^{228}*Th* α*-source peak for each p-side channel of DSSSD "PS32NS32-H".*

Table 3 shows the average p-side energy resolution for each of the tested DSSSD together with the leakage current during each measurement.

Table 3: *Average energy resolution for p-side DSSSDs measured using* ^{228}*Th* α*-source. The energy resolution was calculated for the 8684.86 keV peak. The leakage current during each measurement is also shown.*

DSSSD	Resolution	Leakage Current [nA]
PS32NS32-H	58.7 keV - 0.68%	70
PS32NS32-K	66.9 keV - 0.77%	443
PS32NS32-F	59.0 keV - 0.68%	63
D20-15	42.8 keV - 0.49%	458

The energy resolution of the DSSSDs were worse than what was expected, which could be due to vacuum causing α-particles to straggle. Another possible reason could be the noise contribution related to readout electronics. Measurement of the electronic related noise contribution was performed using high precision lab pulser. During this measurement the DSSSD was disconnected from the preamplifier input. Figure 19 shows the energy spectrum of the pure electronics response.

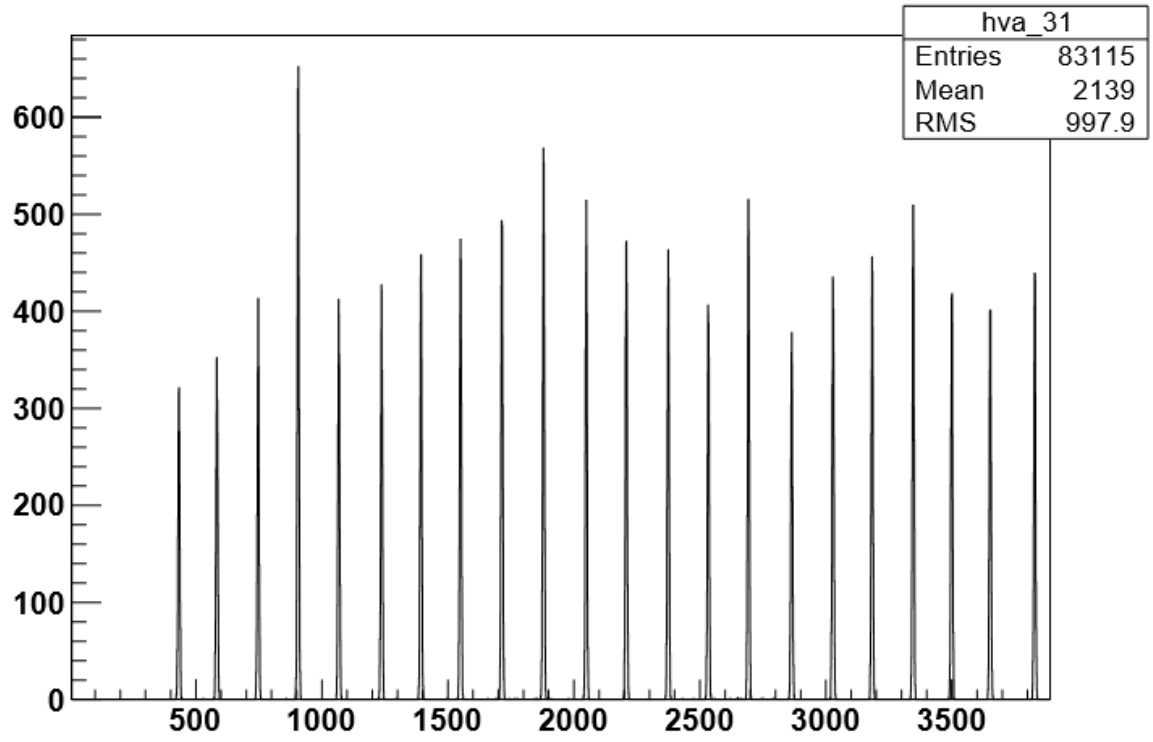

Figure 19: *Energy spectrum of the electronics measurement done using a pulser.*

Measurements of the electronics related noise allows to test the linearity of the readout system. Figure 20 shows the ADC channel number as a function of pulser signal sent to preamplifier test input. It is clear that linearity of the readout system is satisfactory.

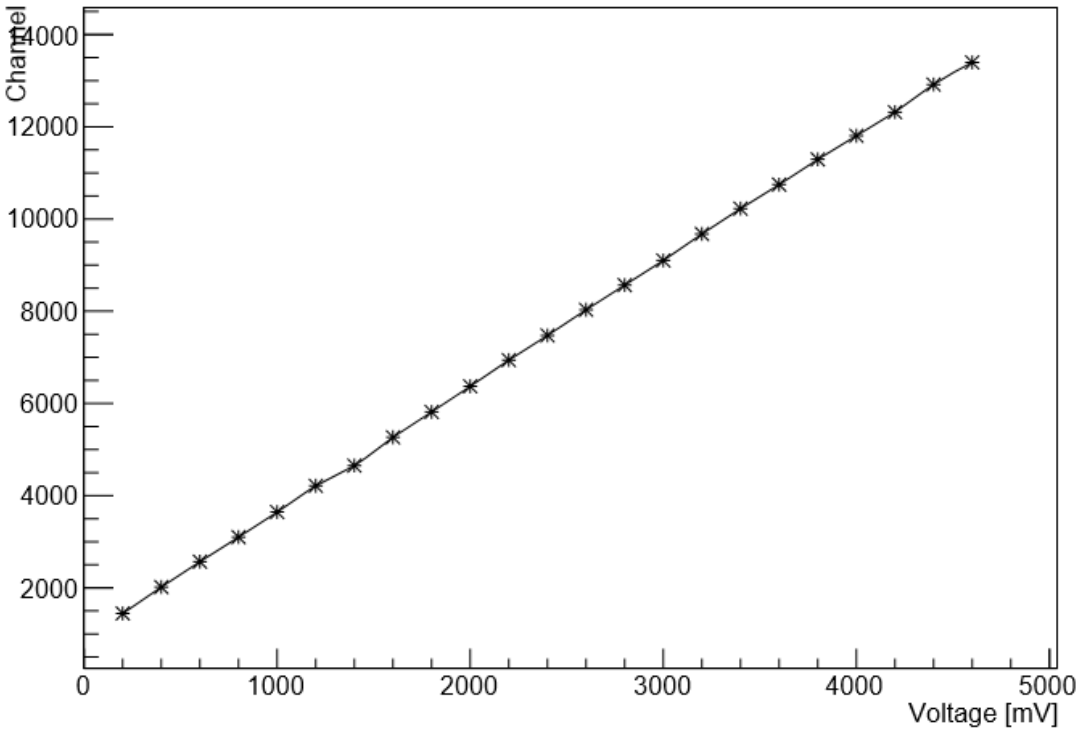

Figure 20: *Linearity measurement using a high precision lab pulser. ADC channel number displayed as a function of pulser signal sent to preamplifier test input.*

The energy resolution of the electronics was found to be between 20-30 keV, as seen in Figure 21. As shown in Figure 21 the pure electronics related noise contribution is not uniform across the readout channels. This spread in electronics noise across the readout channels could be the reason of the difference in energy resolution across the DSSSD channels, which can be seen in Figure 18.

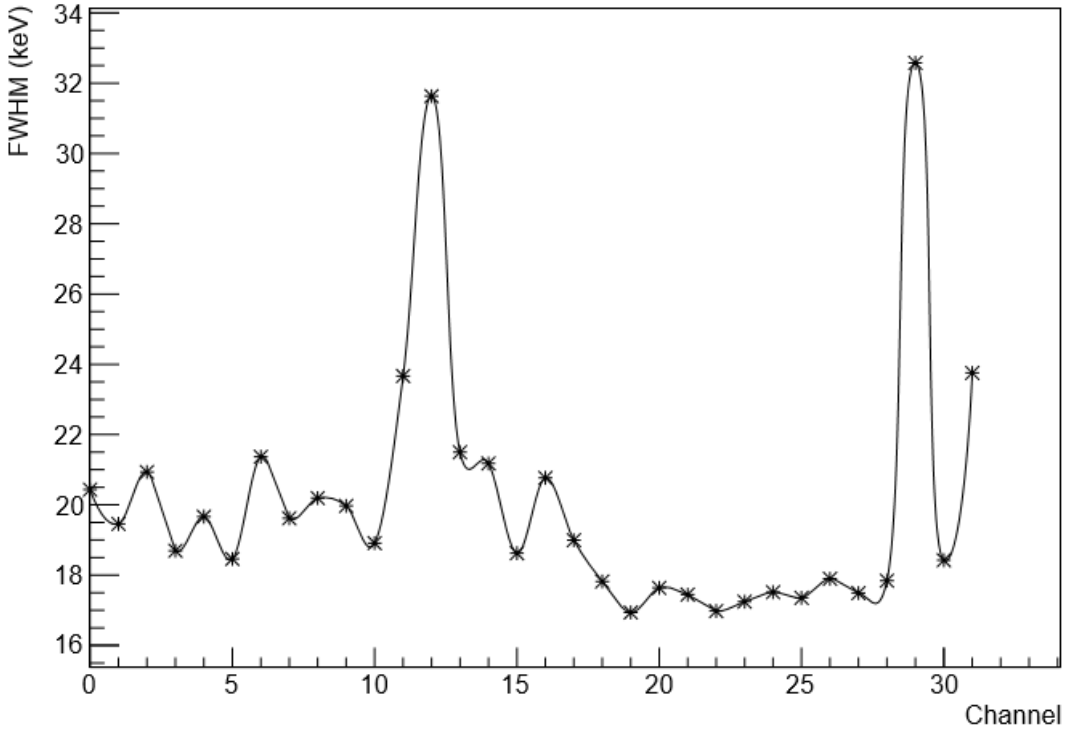

Figure 21: *Energy resolution of the electronics measured using a pulser.*

Another source of uncertainty could be the rather long time of the measurements. The measurements lasted for roughly 12 hours. The temperature variations throughout the long period of time can affect the electronics, resulting in varying energy resolution. Also the calibration was done strip-by-strip rather than pixel by pixel. This will have contributed to the energy spread as the amount of dead layer that the incoming particles passes through depends on the incident angle with respect to the detector. If a charged particle passes through the detector with an incident angle orthogonal to the detector surface then it will experience a minimum amount of dead layer, compared to a charged particle coming in with an angle different from 90°, which will experience a thicker dead layer, and therefore straggle. This assumes that the dead layer thickness is uniform throughout the area of the detector.

4.1.4 Dead Layer Thickness

The dead layer estimation is done by first measuring the energy difference between peaks of an n-side strip, which can be seen in Figure 22. The extra peaks in Figure 22 are due to small openings on the aluminium metalization. These small openings cause some of the incoming radiation to pass through to the detector without depositing energy in the dead layer, which means that two peaks will be measured with a difference in energy corresponding to the energy deposited in the aluminium dead layer. The aluminium openings are positioned along one n-strip on each p-side strip. This results in a fraction of the incoming radiation passing through the openings. However, this fraction is small and will be the same for each p-side strip. The n-side strips are orthogonal to the p-side strip which means that one n-side strip will have a larger fraction of incident radiation passing through the openings, as it is placed directly behind the openings.

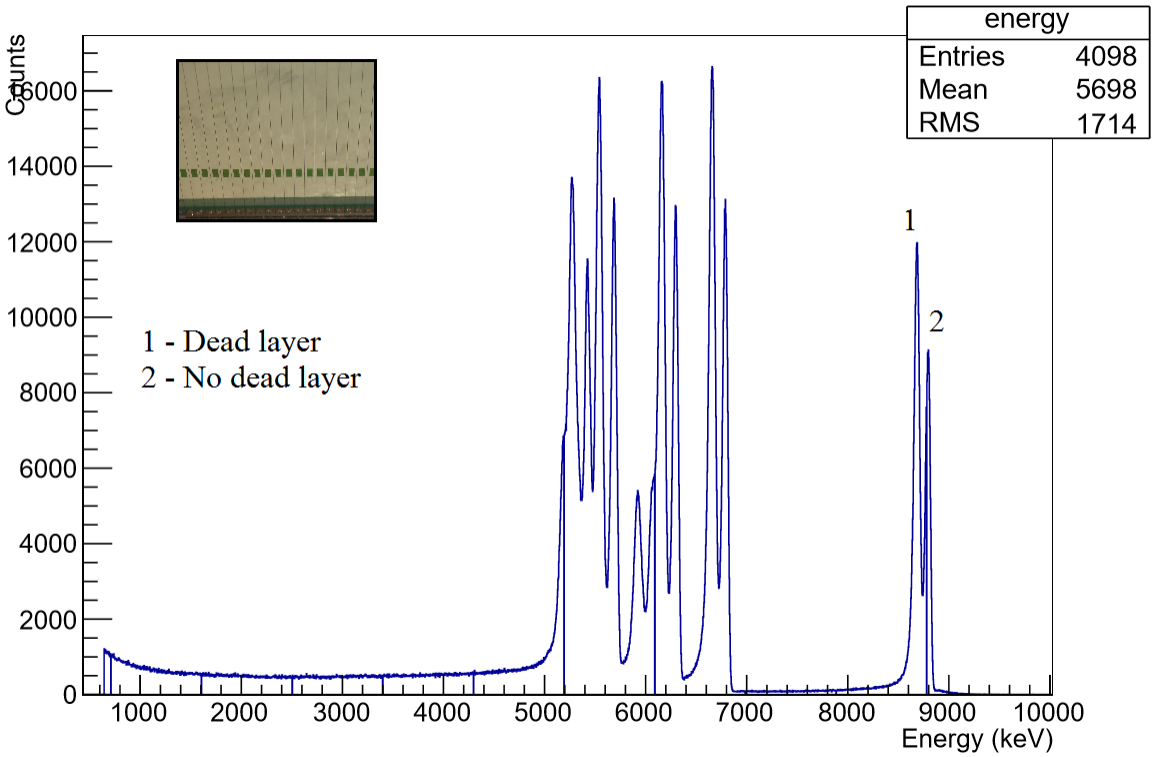

Figure 22: *Energy spectrum of n-side Channel 17 for DSSSD "PS32NS32-H". Top left corner shows the aluminium openings (green) on the p-side on a DSSSD.*

In order to estimate the dead layer thickness one calculates the energy deposition of α-particles, using Equation 1, into the silicon and makes a discrete approximation $\frac{\Delta E}{\Delta x}$. The energy is deposited in aluminium, but the dead layer thickness is calculated for silicon. This is referred to as silicon equivalent. By taking the difference one finds the ΔE and by dividing it by the calculated energy deposition, as show in Equation 6, one can find the dead layer thickness.

$$\frac{\Delta E}{\left(\frac{\Delta E}{\Delta x}\right)} = \Delta x \tag{6}$$

In order to use the properly resolved peaks, only peaks with more than 8000 counts in height, from the measurement presented in Figure 22, are used in the dead layer estimation. The energy difference was calculated by fitting gaussian to each peak and subtracting their positions. Table 4 shows the measured ΔE, calculated $\frac{\Delta E}{\Delta x}$ and corresponding dead layer estimation.

Table 4: *Measured and calculated data used to estimate the dead layer thickness.*

Peak Energy [keV]	ΔE [keV]	$\frac{\Delta E}{\Delta x}$ [keV/μm]	Dead Layer Thickness [μm]
5423	153	150	1.02
5685	145	146	0.99
6288	136	136	1.00
6778	125	129	0.97
8785	101	107	0.94

As Table 4 shows, the dead layer thickness is estimated to be 1.0 μm in silicon equivalent. No error was calculated as the error was believed to be low and it is a crude measurement in order to get a rough estimate of the dead layer.

4.2 CsI(Tl) Detector Testing

The CsI(Tl) detector measurements are done using a ^{228}Th α-source. The source is placed 95 mm away from the CsI(Tl) detector, and is centered to the front of the detector. The measurement is done in the

vacuum chamber and a reverse bias of 50 V is applied to the photodiode. The data analysis is based on acquired ^{228}Th energy spectrum.

4.2.1 Energy Spectrum

The precise energy calibration of CsI(Tl) detectors is not performed due to pure energy resolution for α-particles emitted by ^{228}Th α-source. Figure 23 and 24 shows the energy spectrum for two different channels from the ^{228}Th α-source measurement.

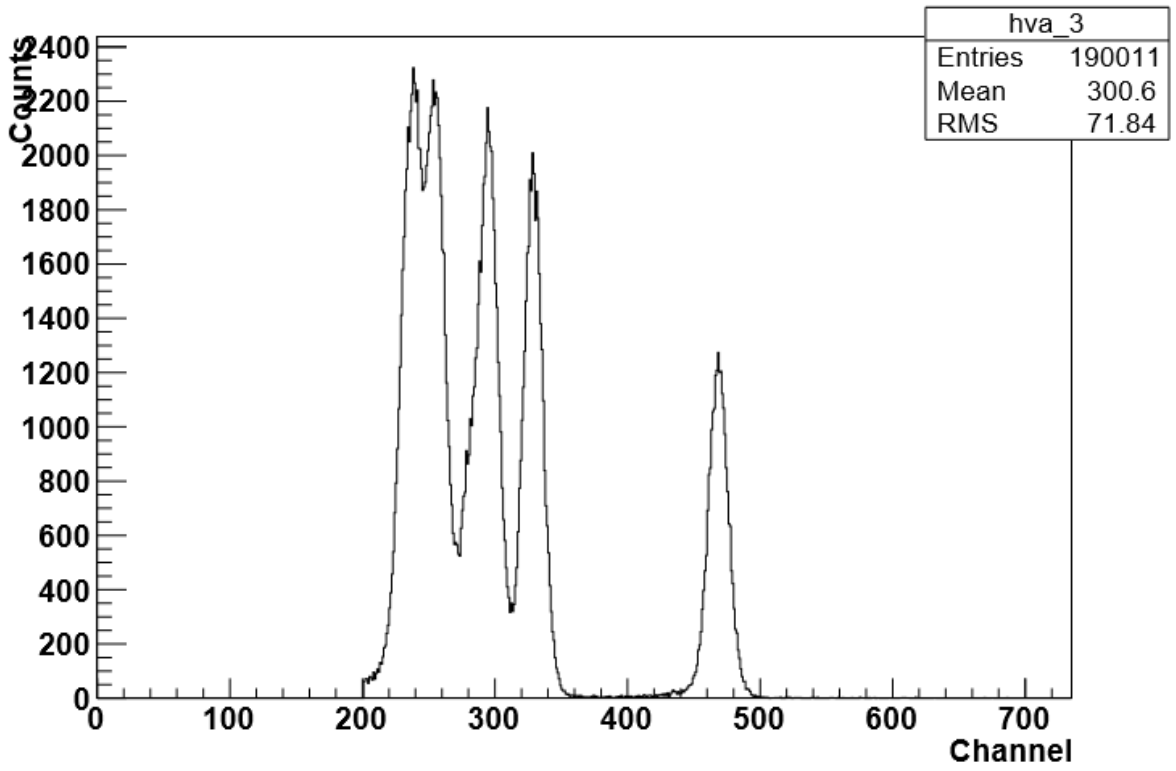

Figure 23: *Energy spectrum for Channel 4 of the CsI(Tl) measurement. Note that the spectrum has been zoomed in, the full spectrum consists of 4096 channels.*

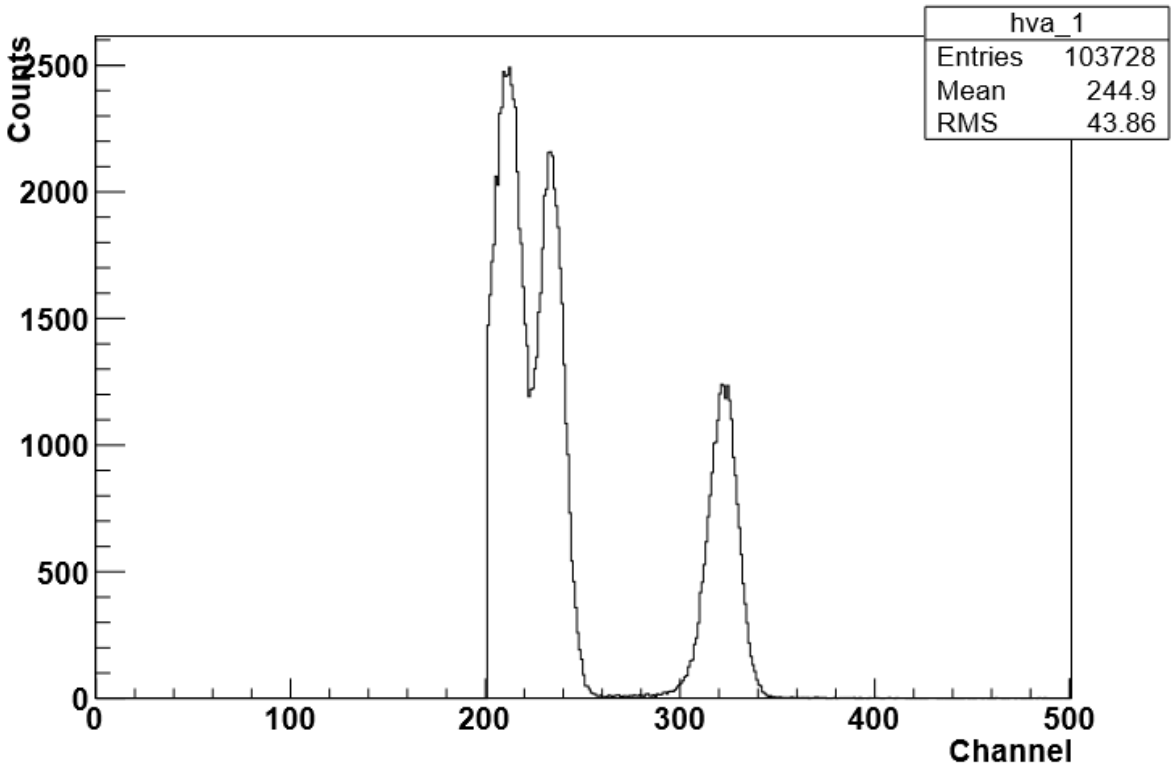

Figure 24: *Energy spectrum for Channel 2 of the CsI(Tl) measurement. Note that the spectrum has been zoomed in, the full spectrum consists of 4096 channels.*

There is an obvious cut off at around Channel 200 at the spectrum in Figure 24. Comparing Figure 23 and 24 one can see a clear difference, Channel 4 can resolve four peaks, Channel 2 can only resolve three peaks. The remaining ^{228}Th α-source peaks have been cut off as their energies are below the threshhold of the MSCF-16.

5 Summary and Outlook

During this bachelor project four LYCCA DSSSDs and one CsI(Tl) detector were successfully tested. The detectors were tested using a dedicated experimental setup. The setup consists of a stainless steel vacuum chamber, vacuum pump, readout electronics and DAQ. CSP-32 charge sensitive preamplifiers and MSCF-16s for pulse shaping and trigger requests. For digitization CAEN V.785 ADCs and CAEN V.775 TDCs are used. The DAQ is controlled remotely by a computer via an optical link. The DAQ software uses C++ with ROOT libraries. The DSSSD measurements and data analysis consists of ^{228}Th α-source energy spectrum, energy resolution and dead layer estimation. The CsI(Tl) detector measurements and data analysis consists of ^{228}Th α-source energy spectrum. All data analysis was done in ROOT.

The energy measurement of the ^{228}Th α-source peaks agreed very well with reference data. However the relative intensities were a bit lower than expected, which most likely due to the method used for calculating the counts in each peak. The leakage current of two DSSSDs were significantly higher than anticipated and might need to be replaced before future experiments at FAIR. The average energy resolution for the DSSSDs was found to be around 0.7% at 8785 keV. The energy resolution of the DSSSDs were not as good as anticipated. This was most likely due to temperature variations during the measurement along with the strip-by-strip calibration. Better energy resolutions of the DSSSDs can be obtained by performing pixel-by-pixel calibrations. The dead layer thickness on the DSSSD p-side is estimated to be on the order of 1 μm silicon equivalent. Testing a CsI(Tl) detector show satisfactory results with low energy α-source. The α-spectrum is resolved and main peaks are visible.

The next step of this project would be to perform pixel-by-pixel calibration of the DSSSDs. This would improve the energy resolution and enable dead layer estimations using the p-side pixels which as the

aluminium openings. Also in-beam verification and detector commissioning are planned in the near future.

6 Appendix A: Data Analysis Script I

```
{
 #include "XEvent.h"
 #include "ScalerEvent.h"
  //#include "Experiment.h"
 int nbin = 4096;
 int xmin = 0;
 int xmax = 4096;
 int files =4; //between 1 and 64 for current data
 int i;
 int maxheight;
 int maxposition;
 int peakwidth;

 int peaks[6];
 //peaks[0]=5340; //Th228
 peaks[0]=5423; //Th228
 peaks[1]=5685; //Ra224
 peaks[2]=6051; //Bi212
 peaks[3]=6288; //Rn220
 peaks[4]=6778; //Po216
 peaks[5]=8785; //Po212

 int threshhold_height;
 //int threshhold_height=40;
 int threshhold_width=30;
 int pulsar_threshhold_height=50;
 int pulsar_threshhold_width=100;
 int n;
 int min=500;
 int detector;
 int pulsarpeak;
 int fwhmpeak;

 Double_t peak_height[files][7];
 Double_t peak_position[files][7];
 Double_t peak_sigma[files][7];
 Double_t position[files][7];
 Double_t error[files][7];
 Double_t area[files][7];

 Double_t pulsar_height[files][25];
 Double_t pulsar_position[files][25];
 Double_t pulsar_sigma[files][25];
 Double_t pulsar_error[files][25];
 Double_t pulsar_position[files][25];
 Double_t pulsar_volt[files][25];

 char hvas [20];
 Double_t strip[files], ht[files], pt[files], wt[files];

 //For electronics energy resolution
 TFile* pulsar_file = TFile::Open("Data165.root");

//%%%%%%%%%%%%%%%%%%%%%%%%%
 //choose detector
 //1-PS32NS32-H
```

```
//2-PS32NS32-K
//3-PS32NS32-F
//4-D20-15

detector=1;
fwhmpeak=5;//choose which peak is being represented in the plot
pulsarpeak=9;

if(detector==1){
threshhold_height=8000;
TFile* test = TFile::Open("Data180.root");// no degraer
//maxheight=32000 ish
}
if(detector==2){
   threshhold_height=500;
   TFile* test = TFile::Open("Data194.root");
   //maxheight=5000 ish
}
 if(detector==3){
    threshhold_height=500;
    TFile* test = TFile::Open("Data207.root");
    //maxheight=1000 ish
}
 if(detector==4){

    threshhold_height=50;
    TFile* test = TFile::Open("Data210.root");
}

TFile* write_file = new TFile("output.root", "RECREATE");

for(i=0; i<files; i++){

sprintf(hvas,"%s%d","hva_",i);

TH1F* histo =new TH1F("histo","histo title",nbin,xmin,xmax);
TH1F* pulsar=new TH1F("pulsar","pulsar title",nbin,xmin,xmax);

histo=(TH1F*)test.Get(hvas);
pulsar=(TH1F*)pulsar_file.Get(hvas);

histo -> GetXaxis()->SetTitle("Channel");
histo -> GetYaxis()->SetTitle("Counts");


//peakfinder alpha source
int nbins = histo->GetSize();
maxheight=threshhold_height;
maxposition=5000;
n=0;

for (int bin=min;bin<nbins;bin++){
 if(histo->GetBinContent(bin)>maxheight){
   maxheight=histo->GetBinContent(bin);
   maxposition=bin;
}
 if(histo->GetBinContent(bin)<threshhold_height){
   if(((bin-maxposition)>threshhold_width)){
```

```
       //printf("%d\n",maxposition);
     if(n<1){
       peakwidth=20;
     }
     if(n>0){
       peakwidth=30;
     }
 TF1* peakfit_1= new TF1("peakfit_1","[3]+[0]*exp(-((x-[1])^2)/(2*[2]^2))",
 maxposition-peakwidth,maxposition+peakwidth);
 //TF1* peakfit_1= new TF1("peakfit_1","[0]*exp(-((x-[1])^2)/(2*[2]^2))",
 maxposition-peakwidth,maxposition+peakwidth);

peakfit_1->SetParName(0,"Height");
peakfit_1->SetParameter(0,maxheight);
peakfit_1->SetParName(1,"Position");
peakfit_1->SetParameter(1,maxposition);
peakfit_1->SetParName(2,"Width");
peakfit_1->SetParameter(2,10);

histo->Fit("peakfit_1","+r");
peak_height[i][n]=peakfit_1->GetParameter(0);//height
peak_position[i][n]=peakfit_1->GetParameter(1);//position
peak_sigma[i][n]=peakfit_1->GetParameter(2);

//peak-ratio calculation
   area[i][n]=0;
   for(int t=0;t<5*(peak_sigma[i][n]);t++){
   area[i][n]=area[i][n]+histo->GetBinContent(
   peak_position[i][n]+t-2.5*peak_sigma[i][n]);
}
n=n+1;
//printf("%d\n",maxposition);
//printf("%s%d\n","n=",n);
maxposition=5000;
maxheight=threshhold_height;
  }
 }
}


//peakfinder pulsar source
maxheight=pulsar_threshhold_height;
maxposition=5000;
n=0;
peakwidth=10;

for (int bin=0;bin<nbins;bin++){
 if(pulsar->GetBinContent(bin)>maxheight){
   maxheight=pulsar->GetBinContent(bin);
   maxposition=bin;
}
 if(pulsar->GetBinContent(bin)<pulsar_threshhold_height){
   if(((bin-maxposition)>pulsar_threshhold_width)){
       printf("%d\n",maxposition);
 TF1* peakfit_1= new TF1("peakfit_1","[0]*exp(-((x-[1])^2)/(2*[2]^2))",
 maxposition-peakwidth,maxposition+peakwidth);
 //TF1* peakfit_1= new TF1("peakfit_1","[0]*exp(-((x-[1])^2)/(2*[2]^2))",
 maxposition-peakwidth,maxposition+peakwidth);
```

```
 peakfit_1->SetParName(0,"Height");
 peakfit_1->SetParLimits(0,100,1000);
 peakfit_1->SetParameter(0,maxheight);
 peakfit_1->SetParName(1,"Position");
 peakfit_1->SetParameter(1,maxposition);
 peakfit_1->SetParName(2,"Width");
 peakfit_1->SetParameter(2,10);
 peakfit_1->SetParLimits(2,1,10);

 pulsar->Fit("peakfit_1","r");
 pulsar_height[i][n]=peakfit_1->GetParameter(0);//height
 pulsar_position[i][n]=peakfit_1->GetParameter(1);//position
 pulsar_sigma[i][n]=peakfit_1->GetParameter(2);
 pulsar_volt[i][n]=200+200*n;


 n=n+1;
 printf("%s%d\n","n=",n);
 maxposition=5000;
 maxheight=pulsar_threshhold_height;
   }
  }
 }
 strip[i]=i;
 histo->Draw();
 printf("%d\n",n);


 //linear regression
 Double_t sum_xy=0;
 Double_t sum_xx=0;
 Double_t sum_x=0;
 Double_t sum_y=0;
 int N=6;

 for(int it=0; it<N;it++){
   sum_xy=sum_xy+peak_position[i][it]*peaks[it];
   printf("%f\n",peak_position[i][it]);
 }
 for(int it=0; it<N;it++){
   sum_xx=sum_xx+peak_position[i][it]*peak_position[i][it];
 }
 for(int it=0; it<N;it++){
   sum_x=sum_x+peak_position[i][it];
 }
 for(int it=0; it<N;it++){
   sum_y=sum_y+peaks[it];
 }

Double_t b=(N*sum_xy-sum_x*sum_y)/(N*sum_xx-sum_x*sum_x);
Double_t a=(sum_y-b*sum_x)/N;
 printf("%f\n%e\n",a,b);


 //resizing
 TH1F * energy = new TH1F("energy","title",nbins,0,a+b*nbins);
 for (int o=0;o<nbins;o++){
```

```
  double y= histo->GetBinContent(o);
  double x= histo->GetBin(o);
  double xnew=a+o*b;
  energy->Fill(xnew,y);
 }

 for(int t=0;t<N;t++){
  position[i][t]=peak_position[i][t]*b+a;
  error[i][t]=peak_sigma[i][t]*b*2.35482;
 }
 for(int t=0;t<n;t++){
  pulsar_position[i][t]=pulsar_position[i][t]*b+a;
  pulsar_error[i][t]=pulsar_sigma[i][t]*b*2.35482;
 }

 //save histograms
 histo->Write();
 energy->Write();
 //end of strip loop (Int i)
 }
 energy -> GetXaxis()->SetTitle("Energy (keV)");
 energy -> GetYaxis()->SetTitle("Counts");
 pulsar -> GetXaxis()->SetTitle("Channel");
 pulsar -> GetYaxis()->SetTitle("Counts");
 energy->Draw();
 //histo->Draw();
 pulsar->Draw();

 Double_t perror[files];
 for(int pol=0;pol<files;pol++){
  perror[pol]=error[pol][fwhmpeak];
 }

 Double_t pulerror[files];
 for(int pol=0;pol<files;pol++){
     if(pulsar_error[pol][pulsarpeak]>0){
        pulerror[pol]=pulsar_error[pol][pulsarpeak];
     }
     if(pulsar_error[pol][pulsarpeak]<0){
         pulerror[pol]=-1*pulsar_error[pol][pulsarpeak];
     }
 }

 Double_t deterror[files];
for(int pol=0;pol<files;pol++){
    deterror[pol]=sqrt(perror[pol]*perror[pol]-pulerror[pol]*pulerror[pol]);
    //deterror[pol]=perror[pol]-pulerror[pol];
}
int pulsarpeaks=23;
Double_t pulsarvolt[pulsarpeaks];
Double_t pulsarposition[pulsarpeaks];
for(int pol=0;pol<pulsarpeaks;pol++){
    pulsarvolt[pol]=pulsar_volt[3][pol];
    pulsarposition[pol]=pulsar_position[3][pol];
}
TGraph *volts=new TGraph(pulsarpeaks,pulsarvolt,pulsarposition);
volts->GetXaxis()->SetTitle("Voltage [mV]");
volts->GetYaxis()->SetTitle("Channel");
```

```
volts->Draw("AC*");

 Double_t peakarea[N];
 Double_t nn[N];
 for(int t=0;t<N;t++){
    peakarea[t]=area[2][t];
    printf("%f\n",peakarea[t]);
    printf("%f\n",peakarea[t]/peakarea[0]);
    nn[t]=t;
 }
 TGraph *areas = new TGraph(N,nn,peakarea);
 areas -> GetXaxis()->SetTitle("Peak");
 areas -> GetYaxis()->SetTitle("Counts");
 //areas->Draw("AC*");

 TGraph * fwhm = new TGraph(files,strip,perror);
 fwhm -> GetXaxis()->SetTitle("Channel");
 fwhm -> GetYaxis()->SetTitle("FWHM (keV)");
 //fwhm->Draw("AC*");

 TGraph * pulse_fwhm = new TGraph(files,strip,pulerror);
 pulse_fwhm -> GetXaxis()->SetTitle("Channel");
 pulse_fwhm -> GetYaxis()->SetTitle("FWHM (keV)");
// pulse_fwhm->Draw("AC*");

 TGraph * detector_fwhm = new TGraph(files,strip,deterror);
 detector_fwhm -> GetXaxis()->SetTitle("Channel");
 detector_fwhm -> GetYaxis()->SetTitle("FWHM (keV)");
 //detector_fwhm->Draw("AC*");

 Double_t avg=0;
 for(int i=0;i<files;i++){
     avg=avg+perror[i]/files;
 }
 printf("%f\n",avg);
}
```

7 Appendix B: Data Analysis Script II

```
{
 int nbin = 4096;
 int xmin = 0;
 int xmax = 4096;
 int i;
 int maxheight;
 int maxposition;
 int peakwidth;

 int peaks[5];
 //peaks[0]=5340; //Th228
 peaks[0]=5423; //Th228
 peaks[1]=5685; //Ra224
 //peaks[2]=6051; //Bi212
 peaks[2]=6288; //Rn220
 peaks[3]=6778; //Po216
 peaks[4]=8785; //Po212

 int threshhold_height=6000;
```

```
 int threshhold_width=10;
 int n;
 int min=500;

 Double_t peak_height[10];
 Double_t peak_position[10];
 Double_t peak_sigma[10];
 Double_t position[10];
 Double_t error[10];
 char hvas [20];

//%%%%%%%%%%%%%%%%%%%%%%%%

 TFile* test = TFile::Open("Data180.root");// no degraer
 TFile* write_file = new TFile("output.root", "RECREATE");

 TH1F* histo =new TH1F("histo","histo title",nbin,xmin,xmax);
 histo=(TH1F*)test.Get("hva_57");
 histo -> GetXaxis()->SetTitle("Channel");
 histo -> GetYaxis()->SetTitle("Counts");

 //peakfinder
 int nbins = histo->GetSize();
 maxheight=threshhold_height;
 maxposition=5000;
 n=0;

 for (int bin=min;bin<nbins;bin++){
  if(histo->GetBinContent(bin)>maxheight){
    maxheight=histo->GetBinContent(bin);
    maxposition=bin;
 }
  if(histo->GetBinContent(bin)<threshhold_height){
    if(((bin-maxposition)>threshhold_width)){
      if(n<2){
peakwidth=20;
      }
      else{
peakwidth=40;
      }
  TF1* peakfit_1= new TF1("peakfit_1","[3]+[0]*exp(-((x-[1])^2)/(2*[2]^2))",
  maxposition-peakwidth,maxposition+peakwidth);

 peakfit_1->SetParName(0,"Height");
 peakfit_1->SetParameter(0,maxheight);
 peakfit_1->SetParName(1,"Position");
 peakfit_1->SetParameter(1,maxposition);
 peakfit_1->SetParName(2,"Width");
 peakfit_1->SetParameter(2,10);
 histo->Fit("peakfit_1","+r");

 peak_height[n]=peakfit_1->GetParameter(0);//height
 peak_position[n]=peakfit_1->GetParameter(1);//position
 peak_sigma[n]=peakfit_1->GetParameter(2);

 n=n+1;
 printf("%d\n",maxposition);
```

```
 maxposition=5000;
 maxheight=threshhold_height;
   }
  }
 }

 histo->Draw();
 printf("%d\n",n);


 //linear regression
 Double_t sum_xy=0;
 Double_t sum_xx=0;
 Double_t sum_x=0;
 Double_t sum_y=0;
 int N=5;

 for(int it=0; it<N;it++){
   sum_xy=sum_xy+peak_position[2*it+1]*peaks[it];
   printf("%d\n",peak_position[2*it+1]);
 }

 for(int it=0; it<N;it++){
   sum_xx=sum_xx+peak_position[2*it+1]*peak_position[2*it+1];
 }
 for(int it=0; it<N;it++){
   sum_x=sum_x+peak_position[2*it+1];
 }
 for(int it=0; it<N;it++){
   sum_y=sum_y+peaks[it];
 }

Double_t b=(N*sum_xy-sum_x*sum_y)/(N*sum_xx-sum_x*sum_x);
Double_t a=(sum_y-b*sum_x)/N;
 printf("%f\n%e\n",a,b);


 //resizing
 TH1F * energy = new TH1F("energy","title",nbins,0,a+b*nbins);
 for (int o=0;o<nbins;o++){
   double y= histo->GetBinContent(o);
   double x= histo->GetBin(o);
   double xnew=a+o*b;
   energy->Fill(xnew,y);
 }

 Double_t position[n];
 Double_t error[n];
  for(int t=0;t<n;t++){
   position[t]=peak_position[t]*b+a;
   error[t]=peak_sigma[t]*b*2.35482;
 }
 //save histograms
 histo->Write();
 energy->Write();
 //end of strip loop (Int i)

 energy -> GetXaxis()->SetTitle("Energy (keV)");
```

```
energy -> GetYaxis()->SetTitle("Counts");
energy->Draw();
//histo->Draw();



Double_t dE[N];
Double_t pk[N];
for(int kl=0;kl<N;kl++){
  dE[kl]=position[2*kl+1]-position[2*kl];
  printf("%f\n",dE[kl]);
  pk[kl]=kl;

TGraph * delta = new TGraph(5,pk,dE);
delta->Draw("AC*");
delta -> GetXaxis()->SetTitle("Peak");
delta -> GetYaxis()->SetTitle("dE [keV]");
}
```

References

[1] http://www.nndc.bnl.gov/chart/ (2017-04-07)

[2] Golubev, P. *et al.*: *The Lund-York-Cologne Calorimeter (LYCCA): Concept, Design and Prototype Developments for a FAIR-NUSTAR Detector System to Discriminate Relativistic Heavy ion Reaction Products* . In print for Nuclear Instruments and Methods in Physics Research Section A.

[3] `https://en.wikipedia.org/wiki/Bethe_formula` (2017-04-07)

[4] `http://www.webexhibits.org/causesofcolor/images/content/30_dec08Z.jpg` (2017-04-28)

[5] Krane, K.S.: *Introductory Nuclear Physics.* Wiley, 1988.

[6] Leo, W.R.: *Techniques for Nuclear and Particle Physics Experiments.* Springer, 1987.

[7] `https://root.cern.ch/` (2017-05-04)

[8] `http://www.mesytec.com/index.html` (2017-05-04)

[9] Rudolph, D. *et al.*: *Technical Report, V1.2, June 2008 LYCCA — the Lund-York-Cologne CAlorimeter Identification of reaction products in HISPEC-DESPEC@NuSTAR.* ?I dont know in which paper it is published?.

[10] `http://www.caen.it/` (2017-05-05)

[11] RADCON Ltd., Zelenograd, Russia

[12] Amcrys-H Ltd., Kharkov, Ukraine

[13] Isotope Products Laboratories, Eckert & Ziegler, Valencia, California. `http://www.ezag.com` (2017-05-08)